

1 ***Toxoplasma gondii* GRA28 is required for placenta-specific induction of the**
2 **regulatory chemokine CCL22 in human and mouse.**

3

4 Elizabeth N. Rudzki¹, Stephanie E. Ander^{1,2}, Rachel S. Coombs¹, Hisham S. Alrubaye¹, Leah F.
5 Cabo¹, Matthew L. Blank¹, Nicolas Gutierrez-Melo¹, JP Dubey³, Carolyn B. Coyne⁴ and Jon P.
6 Boyle^{1*}

7

8 ¹Department of Biological Sciences, Dietrich School of Arts and Sciences, University of
9 Pittsburgh, Pittsburgh, PA. 15260.

10 ²Department of Pediatrics, University of Pittsburgh School of Medicine, Pittsburgh, PA. 15260

11 ³United States Department of Agriculture, Agricultural Research Service, Beltsville Agricultural
12 Research Center, Animal Parasitic Diseases Laboratory, Beltsville, Maryland, 20705.

13 ⁴Department of Molecular Genetics and Microbiology, Duke University School of Medicine,
14 Durham, NC. 27708.

15

16

17 *Author to whom correspondence should be addressed:

18 Jon Patrick Boyle, PhD

19 Associate Professor

20 Department of Biological Sciences

21 Dietrich School of Arts and Sciences

22 University of Pittsburgh

23 4249 Fifth Avenue

24 Pittsburgh, PA. 15260

25 Email: boylej@pitt.edu

26 **ABSTRACT**

27 *Toxoplasma gondii* is an intracellular protozoan pathogen of humans that can cross the placenta
28 and result in adverse pregnancy outcomes and long-term birth defects. The mechanism used by
29 *T. gondii* to cross the placenta are unknown but complex interactions with the host immune
30 response are likely to play a role in dictating infection outcomes during pregnancy. Prior work
31 showed that *T. gondii* infection dramatically and specifically increases the secretion of the
32 immunomodulatory chemokine CCL22 in human placental cells during infection.. Given the
33 important role of this chemokine during pregnancy, we hypothesized that CCL22 induction was
34 driven by a specific *T. gondii*-secreted effector. Using a combination of bioinformatics and
35 molecular genetics, we have now identified *T. gondii* GRA28 as the gene product required for
36 CCL22 induction. GRA28 is secreted into the host cell where it localizes to the nucleus, and
37 deletion of this gene results in reduced CCL22 placental cells as well as a human monocyte cell
38 line. The impact of GRA28 on CCL22 production is also conserved in mouse immune and
39 placental cells both *in vitro* and *in vivo*. Moreover, parasites lacking GRA28 are impaired in their
40 ability to disseminate throughout the animal, suggesting a link between CCL22 induction and
41 the ability of the parasite to cause disease. Overall these data demonstrate a clear function for
42 GRA28 in altering the immunomodulatory landscape during infection of both placental and
43 peripheral immune cells, and show a clear impact of this immunomodulation on infection
44 outcome.

45

46 **AUTHOR SUMMARY**

47 *Toxoplasma gondii* is a globally ubiquitous pathogen that can cause severe disease in
48 HIV/AIDS patients and can also cross the placenta and infect the developing fetus. We have
49 found that placental and immune cells infected with *T. gondii* secrete significant amounts of a
50 chemokine (called “CCL22”) that is critical for immune tolerance during pregnancy. In order to

51 better understand whether this is a response by the host or a process that is driven by the
52 parasite, we have identified a *T. gondii* gene that is absolutely required to induce CCL22
53 production in human cells, indicating that CCL22 production is a process driven almost entirely
54 by the parasite rather than the host. Consistent with its role in immune tolerance, we also found
55 that *T. gondii* parasites lacking this gene are less able to proliferate and disseminate throughout
56 the host. Taken together these data illustrate a direct relationship between CCL22 levels in the
57 infected host and a key parasite effector, and provide an interesting example of how *T. gondii*
58 can directly modulate host signaling pathways in order to facilitate its growth and dissemination.

59 INTRODUCTION

60 *Toxoplasma gondii* is an obligate intracellular parasite that is an important parasite of
61 humans and other animals. While this pathogen is particularly well-known to cause severe
62 disease in the immunocompromised, such as those with HIV/AIDS or undergoing
63 immunosuppression for organ transplants, *T. gondii* is also capable of crossing the placenta and
64 infecting the developing fetus, leading to a variety of infection outcomes ranging from
65 asymptomatic to severe (1). Importantly, even children born without symptoms are at high risk
66 for extensive health problems later in life, including ocular disease and neurological disorders
67 (2, 3). To date little is known about how *T. gondii* gains access to the fetal compartment and
68 how the host responds to the presence of parasites at the maternal-fetal interface.

69 Recently we (4) found that primary human trophoblast cells (derived from term
70 placentas) and 2nd trimester placental explants produced the chemokine CCL22 in response to
71 infection with *T. gondii* (4). Production of this chemokine was dependent on parasite invasion
72 and the dense granule effector trafficking gene product MYR1 (4). While the role of CCL22
73 during infection with *T. gondii* is poorly understood, this chemokine is a key molecular signal for
74 the recruitment of regulatory T cells which are well known for their role in suppressing immune
75 responses to tumors, leading to poor clinical outcomes (5, 6). Importantly disruption of T_{reg}

76 recruitment to tumors can lead to improved outcomes in animal models. For example, using
77 *Ccl22* DNA vaccines in mice leads to misdirection of regulatory T cells and ultimately reduced
78 tumor growth (5). The role for CCL22 in healthy humans is less well understood, although it is
79 thought to subvert and/or modulate inflammatory responses and may be particularly important
80 for response resolution after pathogen clearance. CCL22 and regulatory T cells also play a
81 critical role during pregnancy, where they seem to govern immune tolerance (7) and regulation
82 of inflammation at the maternal-fetal interface. This regulatory role appears to be critical in
83 determining pregnancy outcome during pathogen-mediated immune activation (7, 8). Given the
84 important role played by CCL22 during pregnancy and our recent findings regarding the ability
85 of a congenitally acquired parasite to directly modulate production of this chemokine, we sought
86 to identify the parasite effector(s) responsible for this in order to determine the impact of CCL22
87 modulation on congenital transmission and pregnancy outcome during vertical transmission. To
88 do this we used a bioinformatic screen identify candidate genes and identified one
89 (TGGT1_231960) as being required for CCL22 induction in human and mouse cells. Overall
90 these data show that a specific effector is largely responsible for *T. gondii*-mediated CCL22
91 induction in a relatively small number of human and mouse cell types, and suggest that the
92 manipulation of CCL22 levels by GRA28 may influence the ability of *T. gondii* to disseminate to
93 throughout the host.

94

95 RESULTS

96 ***Toxoplasma gondii* induces a monocyte-like cell line to produce the** 97 **immunomodulatory chemokine CCL22.**

98 Previous work established that placental explants and primary human trophoblasts infected with
99 *T. gondii* had increased *CCL22* transcript abundance and released more CCL22 protein into the
100 culture media compared to mock infected controls (4). Since we also found that not all cell types

101 produce CCL22 in response to infection (e.g., HFFs), we were interested in identifying a human
102 cell line that could be used as a more tractable model than placental cells to assay *T. gondii*-
103 driven CCL22 induction. THP-1 cells, a cell line derived from a patient with monocytic leukemia,
104 were a reasonable candidate given their origins in the myeloid lineage and known production of
105 CCL22 in response to a variety of stimuli (9, 10). We infected THP-1 cells with a type 1 *T. gondii*
106 strain (RH88 or RH:YFP;(4)) at a multiplicity of infection (MOI) of 3. Following 24 hours of
107 infection, supernatants were collected from each well. Human foreskin fibroblasts (HFFs) were
108 infected in parallel as negative controls. Mock treatments involved passing the parasite solution
109 through a 0.22 μ M filter prior to exposure to the cells. Based on CCL22 ELISA, *T. gondii*
110 infection induced CCL22 in THP-1 cells, and as expected there was no CCL22 production from
111 mock-treated controls or *T. gondii*-infected HFFs (**Figure 1a**). We also infected primary
112 placental tissues in the same manner, and as expected villous tree explants and decidua taken
113 from 2nd trimester placentas produced significantly more CCL22 compared to mock-treated
114 controls (**Figure 1a**). In addition to the type 1 RH strain, other *T. gondii* strain types (Type
115 2:PRU and Type 3:CEP; Supplementary **Figure 1 Supplement 1a**) also induced secretion of
116 CCL22 from THP-1 cells, as did the nearest extant relative of *T. gondii*, *Hammondia hammondi*
117 (**Figure 1 Supplement 1b**). In contrast to *H. hammondi*, and just as we observed previously in
118 primary human placental cells (4), *Neospora caninum* has no effect on THP-1 production of
119 CCL22 (Supplementary **Figure 1 Supplement 1b**). These data provided strong support that the
120 mechanism of CCL22 induction was the same for THP-1 and placental cells.

121 We also determined if live parasites were required to induce CCL22 in THP-1 cells by
122 exposing host cells to parasites that were exposed to a variety of lethal treatments. As shown in
123 **Figure 1b** dead parasites failed to induce CCL22 production by THP-1 cells. We also pretreated
124 parasites and host cells with 10 μ g/mL Cytochalasin-D (Cyt-D) to block invasion (11), and as
125 shown in **Figure 1c** Cyt-D treated parasites were significantly impaired in their ability to induce
126 CCL22, suggesting that active invasion was required for this phenomenon. We obtained similar

127 results with the inhibitor 4-BPB (**Figure 1d**), which also significantly blocked CCL22 production
128 by THP-1 cells at 0.5 and 1 μ M. This drug blocks rhoptry and dense granule secretion from *T.*
129 *gondii*, but not microneme secretion(12), suggesting that the factor is not a microneme protein
130 (**Figure 1d**). We also infected THP-1 cells with *T. gondii* parasites that were deficient in the
131 dense granule trafficking protein MYR1 ((13); kind gift from John Boothroyd, Stanford
132 University) and compared them to TgRH Δ MYR1:MYR1_c parasites. TgRH Δ MYR1 parasites
133 failed to induce any detectable CCL22 from THP-1 cells while, as expected,
134 TgRH Δ MYR1:MYR1_c parasites induced significantly more than mock-treated cells (**Figure 1e**).
135 We also observed a very tight correlation between parasite multiplicity of infection (MOI) and
136 CCL22 levels, suggesting that the signal was primarily driven by the parasite rather than the
137 host cell (**Figure 1f**). Based on these results we felt confident that the unknown secreted factor
138 driving CCL22 production in human primary placental cells was very likely the same as the one
139 driving it in the THP-1 cell line and chose THP-1 cells for screening candidate effectors given
140 their tractability in the laboratory.

141

142 **Transcript abundance correlation analysis identifies a large group of putatively** 143 **MYR1-trafficked gene products.**

144 As described previously (above and (4)), we have determined that primary human trophoblast
145 cells infected with *T. gondii* have a transcriptional signature that is characterized by the
146 production of immunomodulatory chemokines, with CCL22 being the most potently induced. To
147 identify candidate *T. gondii* genes responsible for this effect on placental cells, and since this
148 effect required the *T. gondii* effector translocation complex protein MYR1 (4), we hypothesized
149 that MYR1-dependent substrates would have highly correlated gene expression profiles across
150 diverse gene expression datasets. To test this hypothesis, we generated an “all vs. all”
151 correlation matrix of 396 *T. gondii* Affymetrix microarray datasets that we downloaded and

152 curated from the Gene Expression Omnibus (see Materials and Methods). Analysis of the entire
153 correlation matrix (shown in **Figure 2a** and downloadable at 10.6084/m9.figshare.16451832)
154 confirms this hypothesis for certain gene classes. For example, we identified one cluster
155 containing multiple SAG-related sequences (SRS) which are typically expressed at high levels
156 in bradyzoites (including SRS49 cluster members A, C and D; **Figure 2 Supplement 1A**) and
157 another containing 70 genes, 43 of which encode ribosomal subunits (**Figure 2 Supplement**
158 **1a**). Examination of the gene expression heatmaps across all 396 microarray analyses clearly
159 show distinct patterns of gene expression in these two clusters depending on life stage
160 treatment exposure (**Figure 2 Supplement 1a,b**).

161 We quantified the degree of transcript abundance correlation between 5 “bait” genes
162 (*MYR1*, 2 and 3; (13, 14)) and the known *MYR1*-dependent substrates *TgGRA24* and *TgIST*
163 (15, 16)) and all other genes across all 396 expression datasets. We identified genes as
164 candidate *MYR1* substrates if they had an average correlation with the 5 “bait” genes ≥ 0.7 , a
165 dN/dS ratio ≥ 2 , and the presence of a predicted signal peptide OR at least one transmembrane
166 domain. Using this set of filters we were left with 28 candidate genes (plus all 5 bait genes
167 which also met these cutoffs), including the known *TgMYR*-dependent substrate *TgGRA25* (17).
168 Since all known *MYR1* trafficked substrates are dense granule proteins, we eliminated any
169 surface antigens or soluble enzymes, leaving a number of confirmed dense granule proteins
170 (e.g., *GRA4* and *GRA8*) and conserved hypothetical proteins. Importantly, when we examined
171 the correlation between the bait genes and all *T. gondii* genes annotated as “Dense granule”
172 either in the primary product notes or via user annotation, we found that not all dense granule-
173 encoding transcripts correlated highly with bait transcript levels (**Figure 3 Supplement 1a**),
174 indicating that our approach could discriminate between different classes of proteins secreted
175 from the same organelle. For example, while genes like *GRA32* (*TGME49_212300*) had
176 transcript levels with relatively high (>0.8) correlations with bait transcript levels, other genes
177 encoding *GRA1*, *GRA2* and *GRA11* paralogs had transcript levels that correlated much more

178 poorly with the bait genes. This is despite the fact that most of these dense granule encoding
179 genes have high transcript levels compared to other gene clusters as shown in the heat map in
180 **Figure 3 Supplement 1a**, demonstrating that our approach yielded an additional layer of
181 discrimination to categorize dense granule-trafficked gene products. Moreover, many of the co-
182 regulated genes are not yet annotated but based on our analysis one would predict that many
183 are likely to be dense granule protein derived secreted effectors or structural constituents of this
184 parasite organelle.

185

186 ***T. gondii* GRA28 is the gene responsible for CCL22 induction in human immune** 187 **and placental cells.**

188 When we specifically examined correlations between the bait genes listed above and *MYR1*, we
189 found that *MYR1* expression profiles were highly correlated at the transcriptional level with
190 *MYR2/3* and *IST* (**Figure 2b,c** and **Figure 3a**, top), consistent with the idea that *MYR1*
191 substrates could be identified using this approach. After identifying a small list of candidate
192 genes (**Figure 3a**, bottom), we deleted each using CRISPR-CAS9 and screened for CCL22-
193 induction in THP-1 monocytes by ELISA. Among the five genes that we tested (including
194 *GRA18* which was recently found to induce Ccl22 in mouse macrophages; (18)), we found that
195 *GRA28* (*TGME49_231960*) was required for the induction of CCL22 secretion by infected THP-
196 1 monocytes (**Figure 3b**). We also found that Δ *Toxofilin* parasites had significantly reduced
197 levels of CCL22 induction (**Figure 3b**), albeit to a much lesser extent than Δ *GRA28* parasites.
198 We think it likely that this decrease is owed to the reduced invasion capacity of Δ *Toxofilin*
199 parasites rather than a direct impact of this gene product on host CCL22 production (19, 20).

200 To determine if *GRA28* was responsible for CCL22 production by human placental cells,
201 we infected 2nd trimester human villous placental explants with WT and Δ *GRA28* parasites and
202 observed a marked decrease in CCL22 production by explants exposed to Δ *GRA28* parasites

203 compared to WT (**Figure 3c**). To gain a broader understanding of the transcriptional networks
204 altered by *GRA28* we compared THP-1 cells infected with *RHΔHPT:HPT* and *RHΔGRA28* using
205 RNAseq. A relatively small number of transcripts had significantly altered abundance using
206 stringent statistical cutoffs (67 genes with $P_{adj} < 0.0001$ and $abs(\log_2FC) \geq 2$) are highlighted in
207 **Figure 3d**) and these included CCL22 as well as the chemokines XCL1 and XCL2. Interestingly
208 transcript abundance for CCL17, a chemokine that is often co-regulated with CCL22 (21, 22)
209 and which is induced in some cells along with CCL22 by the *T. gondii* effector GRA18 (18), was
210 not dependent on *GRA28* (**Figure 3d**). The majority of transcripts that were *GRA28*-dependent
211 were of higher abundance in WT compared to Δ *GRA28* parasites when using slightly relaxed
212 statistical cutoffs (263 higher, 33 lower; $P_{adj} < 0.05$ and $\log_2FC \geq 1$ or ≤ -1).

213 We performed pathway analysis on these sets of regulated genes using Ingenuity
214 pathway analysis (IPA) and identified host cell pathways that were either more or less induced
215 in WT *T. gondii*-infected cells compared to Δ *GRA28*-infected cells (**Figure 4**), including
216 Dendritic Cell Maturation, IL6 and IL8 signaling, and NFκB signaling (**Figure 4a**). When we
217 assessed the degree of gene overlap in these gene sets, we found that 10 of the pathways
218 contained the *JUN* and *FOS* genes (**Figure 4b**), indicating a potential role for AP-1 complex
219 targeted transcripts in *GRA28*-dependent transcriptional changes. We examined correlations
220 across these gene sets (after creating a matrix of presence/absence of each of the genes
221 shown in **Fig. 4b**) and identified two non-overlapping sets of genes. The larger cluster contains
222 multiple immunity-related genes while the smaller cluster contains genes involved in
223 proteoglycan synthesis (**Figure 4c**), including the *XYLT1* gene which encodes the enzyme that
224 adds UDP-Xylose to serine residues as a first step in glycosaminoglycan synthesis. When we
225 performed a similar analysis using the “upstream regulator” module in IPA, we identified a small
226 set of significant ($Z\text{-score} \geq 2$; $P < 0.001$) regulatory factors that were upstream of the *GRA28*-
227 dependent gene set, including multiple regulators associated with the NFκB pathway (**Figure 4**
228 **Supplement 1a**). Cluster (**Figure 4 Supplement 1b**) and downstream gene overlap (**Figure 4**

229 **Supplement 1c)** analyses further confirmed the *FOS* and *JUN* genes as contributing to the
230 signaling pathways that were GRA28-dependent, while also confirming a putative role for NFκB.
231 For example, the cluster with the most similar target gene overlap contains multiple genes in the
232 NFκB pathway (*NFKBIA*, *NFKB1*, *RELA*) (**Figure 4 Supplement 1c**). However, when we co-
233 transfected HEK293 cells with NFκB luciferase reporter constructs and a construct encoding the
234 first exon of *GRA28* (see below) we saw no increase in the levels of luciferase after GRA28
235 transfection in contrast to a known NFκB activating construct containing multiple Caspase
236 Activation and Recruitment Domains (CARDs; **Figure 4d**). This suggests that NFκB activation
237 may not play a role in CCL22 induction. Other candidate transcriptional mediators with GRA28-
238 dependent transcript levels are *FOS*, *JUN* and *IRF4* (**Figure 4 Supplement 1d**). Transcript
239 levels of *JUN* have been shown in numerous studies to increase in a variety of host cells after
240 infection with *T. gondii* (23, 24). To test whether GRA28 played a role in altering C-JUN
241 abundance during infection we infected THP-1 cells with WT or ΔGRA28 *T. gondii* parasites for
242 24 h and using semi-quantitative western blotting to quantify C-JUN protein levels. While
243 infection of THP-1 cells clearly increased C-JUN levels compared to mock-treated cells (**Figure**
244 **4 Supplement 2**), the presence or absence of GRA28 in the infecting strain had no significant
245 impact on C-JUN protein abundance. These data suggest that while JUN transcript levels
246 appear to be at least somewhat dependent on GRA28 in the infecting strain (**Figure 4**
247 **Supplement 1d**), this does not appear to be detectable at the protein level using western
248 blotting.

249

250 **The first exon of *GRA28* is sufficient for induction of CCL22 in during parasite**
251 **infection of and ectopic expression in human cells.**

252 The *GRA28* gene has been described previously as encoding a dense granule protein that was
253 capable of trafficking to the host cell nucleus during infection (25). However, the exact structure

254 of the GRA28-encoding gene was somewhat ambiguous based on its annotation in ToxoDB.
255 Specifically, while TGME49_231960 is predicted as a single exon gene spanning ~7.4 kb of
256 genomic sequence (**Figure 5a**), the annotated gene is shorter in TGGT1 (**Figure 5a**) and split
257 into two gene products in *T. gondii* strains VEG, FOU, ARI, VAND, MAS, CATPRC2 and P89.
258 The 5' end of the gene was consistently predicted across all annotated genes, including the
259 precise location of the first intron. When we performed *de novo* assembly of the *T. gondii* RH
260 transcriptome, we were unable to identify any assembled transcripts that spanned the entire
261 length of the TGME49_231960 prediction, most likely due to the fact that a 39 bp repeat in
262 between each of these transcripts disrupted the assembly process (repeat consensus
263 sequence: CAGCAGCAGCCACAAGGGWMTGTTGTGCATCAACCACTA; **Figure 5a**). However
264 it should be noted that when we examined recently released Oxford Nanopore long-read single
265 molecule sequencing of *T. gondii* transcripts that are available on ToxoDB.org there are multiple
266 reads that span this repeat region (select Nanopore reads shown in **Figure 5a**), suggesting that
267 the gene is at least similar to that predicted for ME49 in the *Toxoplasma* genome database.
268 Regardless, given the challenges associated with amplifying and cloning this repetitive region
269 we expressed an HA-tagged version of the first exon of GRA28 in *T. gondii* and observed
270 expression within both the parasites and HA signal in the nucleus of infected cells (**Figure 5b**).
271 Importantly, CCL22 induction could be restored in an RHΔGRA28 clone after bulk transfection
272 of the exon 1 GRA28-expression construct prior to infecting THP-1 cells (**Figure 5c**), confirming
273 the role of sequences present in the first exon of GRA28 in driving CCL22 production in human
274 cells. Similar results were obtained when we transiently expressed a construct containing the
275 entire genomic locus for the predicted *T. gondii* GT1 GRA28 gene (light green bar, **Figure 5a**) in
276 RHΔGRA28 parasites (**Figure 5d**). In contrast, when the Exon 1 construct was expressed
277 transiently in *Neospora caninum* (strain NC-1; (26)), we did not observe any HA signal in the
278 infected host cell despite expression of the protein within the parasite (**Figure 5e**). When we
279 quantified host nuclear HA signal intensity (background subtracted and then normalized to

280 staining intensity within the parasite; see Materials and Methods) in infected host cells there was
281 a clear and significant ($P=0.0012$) difference in the amount of HA-derived signal in the host
282 nucleus when TgGRA28 was expressed in *T. gondii* compared to *N. caninum* (**Figure 5**
283 **Supplement 1a**). Close inspection of multiple images suggest that the trafficking of *T. gondii*
284 GRA28 within *N. caninum* itself may be distinct from how it traffics in *T. gondii*. For example HA
285 staining was observed mostly within the parasite for *N. caninum* but could be found both within
286 *T. gondii* and at the vacuole periphery (**Figure 5e** and **Figure 5 Supplement 1**). While clearly
287 *N. caninum* failed to traffic detectable amounts of GRA28 into the host cell, this could be due to
288 a) poor trafficking of the protein within the parasite such that it never gains proper access to
289 vacuolar export machinery components like MYR1 and/or b) poor trafficking from the parasite
290 into the host cell due to incompatibility with the *N. caninum* export machinery. Interestingly *N.*
291 *caninum* does not appear to have an intact *GRA28* gene in its genome (see the synteny map for
292 TGME49_231960 at ToxoDB.org), although it does have a *MYR1* ortholog which has been
293 shown to be sufficient to traffic secreted *T. gondii* proteins into the host nucleus. Finally,
294 GRA28-Exon1 (minus the residues encoding the predicted signal peptide) could be robustly
295 expressed in HeLa cells with a V5 tag where it trafficked to the host cell nucleus (**Figure 5f**) and
296 also was functional when expressed ectopically in THP-1 cells where it induced CCL22
297 secretion (**Figure 5f**).

298

299 **GRA28 induction of Ccl22 is fully conserved in mice.**

300 To determine whether parasite-driven induction of CCL22 is conserved in the murine model, we
301 compared WT and GRA28-deficient (Δ GRA28) parasites for their ability to induce this
302 chemokine *in vitro*, *ex vivo*, and *in vivo*. First, we infected mouse macrophages (RAW 264.7) *in*
303 *vitro* with type 1 strain (RH) *T. gondii* parasites (WT), or (RH) Δ GRA28 *T. gondii* parasites at
304 MOIs of 3. Based on Ccl22 ELISA, mouse macrophages not only release more Ccl22 protein

305 during *T. gondii* infection, but similar to human THP-1 cells this phenotype is also dependent on
306 the presence of *T. gondii* secreted protein GRA28 (**Figure 6a**). Next, we investigated whether
307 primary mouse tissues, specifically mouse placental tissue, also elicit this response to *T. gondii*
308 infection. Embryonic day 12.5 Swiss Webster mouse placentas were halved and distributed into
309 separate treatment groups. These placental explants were then infected *ex vivo* with 2.0×10^6
310 Type 1 strain (RH) *T. gondii* parasites (WT), (RH) Δ GRA28 *T. gondii* parasites, or mock
311 treatment. As shown in **Figure 6b**, primary mouse placental tissue also responds to *T. gondii*
312 infection by releasing Ccl22 protein in a GRA28-dependent manner. RNA was also extracted
313 from the infected placental samples and we performed RNAseq. As shown in **Figure 6c** the
314 number of transcripts that varied in a GRA28-dependent manner was markedly small,
315 suggesting that GRA28 is a highly specific inducer of *Ccl22* in mouse placental explants. Of the
316 three genes with significantly higher transcript levels (*Ccl22*, *Il12rb2*, *Ccr7*) in wild type
317 1nfections as compared to Δ GRA28 infections, *Ccl22* was the most highly induced. These data
318 show conservation of the parasite-driven Ccl22 phenotype 1n primary mouse placental explants
319 at both a protein and transcript level. Finally, we investigated mouse *in vivo* Ccl22 responses to
320 *T. gondii* intraperitoneal infection. Female BALB/cJ mice (n = 3 for each treatment) were
321 infected with WT, Δ GRA28, or mock *T. gondii* treatments. We focused on early, acute infection
322 and performed Ccl22 ELISA on serum (**Figure 6d**) and peritoneal lavage fluid (**Figure 6e**).
323 These suggest *in vivo* Ccl22 protein levels are at least partially dependent on GRA28.
324 Moreover, while there was a significant amount of systemic Ccl22 protein detected in serum of
325 infected mice, even in the Δ GRA28 parasite treatment, Ccl22 was almost undetectable in
326 peritoneal lavage fluid in Δ GRA28-infected mice. Overall, these data indicate the process
327 driving *T. gondii* GRA28 induced Ccl22 is similar, if not the same, in both mice and humans, and
328 that this parasite effector can mediate robust changes in Ccl22 production at the site of infection
329 and systemically.

330

331 **GRA28-deficient parasites have distinct inflammatory and dissemination**
332 **phenotypes in the acute and chronic phases of infection, respectively.**

333 To determine the impact of *T. gondii* GRA28 *in vivo* we indexed differences in mouse behavior
334 relevant to inflammatory responses and quantified differences in infection-induced weight loss
335 and total morbidity after infection of BALB/cJ mice with either RH:WT or RH Δ GRA28 *T. gondii*.
336 We observed no significant differences in morbidity or weight loss (**Figure 7a,b**). However,
337 when we scored (**Figure 7 Supplement 1**) mice over the course of infection as to the extent of
338 inflammation-induced behavioral changes, we observed significantly heightened fur ruffling in
339 the Δ GRA28-infected mice on days 6 and 7 post-infection (**Figure 7c**), despite the fact that
340 mortality was unchanged.

341 We also generated Δ GRA28 parasites in a Type 2 *T. gondii* background that had been
342 previously engineered to express luciferase and GFP (specifically ME49 Δ HPT:LUC; (27, 28)) to
343 permit non-invasive quantification of parasite burden and dissemination over the course of
344 infection. For the ME49 strain infections we observed only minor and non-significant differences
345 in mouse morbidity and weight loss (**Figure 8a,b**). However, during the acute phase of infection
346 we observed slight differences in parasite burden between ME49 Δ HPT:LUC (WT) and
347 ME49 Δ GRA28-infected mice, with burden being significantly *higher* in ME49 Δ GRA28 compared
348 to WT on day 9 post-infection (**Figure 8c**). This difference was not due to experimental variation
349 in parasite input between strains since parasite burden was indistinguishable during the first 6
350 days post-infection (**Figure 8c**). In contrast to these minor differences during the acute phase of
351 infection, we observed more dramatic differences in parasite burden during the later stages of
352 infection. Specifically, quantification of *in vivo* bioluminescence data taken dorsally on days 14
353 and 15 post-infection revealed that WT parasites were of much greater abundance in the brains
354 compared to those infected with ME49 Δ GRA28 (**Figure 8d,e**).

355

356 **DISCUSSION:**

357 *T. gondii*-infected host cells have dramatically altered transcriptomes compared to
358 uninfected cells, and effectors that are secreted from the parasite during invasion drive most,
359 but not all, of these changes (29). To date, the vast majority of these parasite effectors are
360 derived from the dense granule and rhoptry organelles. We previously identified that *T. gondii*
361 induces the production of CCL22 in human placental trophoblasts, while human foreskin
362 fibroblasts do not exhibit this chemokine induction during *T. gondii* infection (4). Additionally, our
363 previous work has shown that this induction required parasite invasion and the effector
364 chaperone-like *T. gondii* gene product MYR1 (4, 13). While *T. gondii* induces CCL22 during
365 infection of a variety of cell types from both mice and humans (18, 30), including at the
366 transcriptional level in mouse brain (31), placental cell CCL22 induction is driven by a highly
367 specific parasite effector, GRA28. CCL22 production is considered to be an indication of M2
368 macrophage polarization, and macrophage polarization has been linked to strain-specific *T.*
369 *gondii* effectors like ROP16 and GRA15 (32). The impact of GRA28 is distinct from these
370 effectors because CCL22 induction occurs similarly in all three canonical strain types, and
371 GRA28 does not alter the expression of other M2-associated genes (such as *IL4*, *IL10*, *IL13* or
372 *ARG1*), in the cell types that we have assayed. The specificity of GRA28 for only a few target
373 genes is novel compared to effectors like GRA15 and ROP16 (24, 33) that alter the abundance
374 of hundreds of transcripts.

375 Transcriptional co-regulation has been used in other systems as a means to identify
376 members of protein complexes (34), but to our knowledge this is the first time this approach has
377 been successfully applied at this scale in *T. gondii*. We used 396 microarray datasets derived
378 from multiple *T. gondii* life stages and experimental manipulations to provide enough variation to
379 better distinguish subclusters within closely-related gene families. Genes encoding dense

380 granule proteins are among the most highly expressed in the *T. gondii* genome, making them
381 more difficult to separate from one another, but they still clustered into two distinct groups with
382 functional themes. The MYR1/GRA28 cluster harbored a handful of known secreted dense
383 granule effectors, while the other contained genes encoding dense granule structural proteins or
384 those that are secreted into the vacuole but do not traffic to the host cell. We anticipate that the
385 former cluster can be exploited further to identify additional MYR1-trafficked, and putatively
386 host-modulating, effectors while the latter has highlighted new candidates important in dense
387 granule structure or function within the parasite. The entire dataset is available for download as
388 a text file at Figshare (doi: 10.6084/m9.figshare.16451832) so that these data can be mined to
389 identify candidates for membership in other critical *T. gondii*-specific protein complexes.

390 *GRA28* was previously shown to encode a dense granule protein secreted from the
391 parasite into the host cell where it trafficked to the host cell nucleus (25), but its impact on the
392 host cell was unknown. Its natural presence in the host nucleus during infection has also been
393 further confirmed using proteomics, where it was found to be one of the more abundant *T.*
394 *gondii* proteins in the nucleus of the infected host cell (35). The fact that it affects the abundance
395 of only a small number of chemokine-encoding genes at the transcriptional level suggests that it
396 modulates transcriptional activity via direct interactions with transcription factors and/or
397 upstream regulatory sequences. Other *T. gondii* effectors traffic to the host nucleus but this is
398 not always critical for function. For example, ROP16 localization to the host cell nucleus is
399 dispensable for its primary function of phosphorylating STAT6 which occurs in the cytoplasm of
400 the host cell (36). Other *T. gondii* effectors like IST (15, 37) and GRA24 (16) function within the
401 host cell nucleus, but many of these mediate changes in hundreds of transcripts via their
402 cooperation with existing transcriptional suppressors (IST; (15, 37)) or activators (GRA24; (16)).
403 It remains to be seen if the function of GRA28 can occur independent of nuclear trafficking or if
404 this ultimate localization is required for chemokine induction, but its specificity for downstream

405 genes raises the interesting hypothesis that it may function directly, possibly as a heterologous
406 transcription factor.

407 The signaling pathway governing GRA28 function is unknown but some clues can be
408 found in our pathway analyses which suggest a role for GRA28 in mediating changes in key
409 immunity-related host cell signaling pathways. The transcription factor genes *JUN*, *FOS* and
410 components of the NFκB complex were consistently linked to the GRA28-dependent host
411 transcripts. LPS is a well-known activator of both NFκB and C-Jun activity in THP-1 cells (38,
412 39), and this can occur via Toll-like receptor activation (40). However *T. gondii* induction of
413 CCL22 was not fully dependent upon host MYD88, since MYD88^(-/-) THP-1 cells still produced
414 significant amounts of CCL22 in response to *T. gondii* infection (**Figure 1 Supplement 1c**). The
415 difference in CCL22 production by the MYD88^(-/-) cells in comparison to the WT cells should also
416 be considered in light of the fact that the cell lines have different origins (and therefore distinct
417 passage histories which could have the more subtle effects shown on CCL22 production after
418 infection). A distinct cluster of GRA28-dependent host genes was identified that encoded gene
419 products involved in proteoglycan synthesis, including the rate-limiting enzyme XYLT1 . *T.*
420 *gondii* attachment to host cells is mediated by interactions between parasite adhesins and host
421 cell surface sulfated proteoglycans (PG) like heparan sulfate (41, 42), and *T. gondii* adheres
422 poorly to cells with genetically or enzymatically depleted levels of surface sulfated proteoglycans
423 (41, 42). Therefore direct and/or indirect modulation of XYLT1 transcript levels by GRA28 may
424 serve to make infected cells susceptible to adhesion, and ultimately invasion, by *T. gondii* or any
425 other pathogens that depend on surface proteoglycans.

426 GRA28 had no impact on transcript levels of the gene encoding CCL17 which is
427 commonly co-regulated along with *CCL22*. Mouse macrophages infected with *T. gondii* produce
428 Ccl17 and Ccl22 and this is due, at least in part, to another *T. gondii* effector GRA18 (18). Using
429 the same *GRA18* knockout lines (kindly provided by the Bougdour lab) we found that GRA18
430 had no impact on CCL22 production at the transcriptional (not shown) or protein (**Figure 4**) level

431 in human THP-1 cells, suggesting that GRA18 and GRA28 have distinct targets. This is also
432 consistent with the observation that Ccl22 induction in RAW macrophages is only partially
433 dependent on GRA18 and β -Catenin signaling, in contrast to Ccl17 and Ccl24. Finally, in our
434 work we used lower MOIs (2-3 here compared to 5-6 in (18)). Regardless, GRA28 appears to
435 be the more potent modulator of Ccl22 production compared to GRA18, while Ccl17 appears to
436 be much more dependent on GRA18. It is exciting to speculate that *T. gondii* GRA28 has
437 evolved to uniquely target CCL22 as a means to gain access to the fetal compartment since this
438 chemokine is potently induced in placental cells and this chemokine plays a role in immune
439 tolerance during pregnancy (7). However, as shown clearly in this study, GRA28 also alters
440 monocyte/macrophage CCL22 production, making it equally plausible that this intricate
441 molecular relationship developed first as a more generalized immune evasion (via suppression)
442 strategy.

443 The role of specific chemokines like CCL22 during *T. gondii* infection is poorly
444 understood but the discovery of *GRA28* allows this to be addressed more directly using *T.*
445 *gondii* Δ *GRA28* parasites from different genetic backgrounds. Hypervirulent *T. gondii* RH strain
446 Δ *GRA28* parasites caused inflammation-related behavioral changes earlier during infection in
447 mice, compared to mice infected with WT parasites, suggesting that GRA28 functions to
448 suppress inflammatory responses (likely due to induction of CCL22 although we did not test this
449 directly). This could arise via GRA28-mediated recruitment and/or activation of regulatory T cells
450 to the site of infection. These behavioral changes occurred without an effect on the acute
451 virulence phenotype as all mice succumbed to the infection with similar kinetics, which is
452 consistent with an impact of GRA28 on suppressing inflammatory responses without altering the
453 ability of the mouse to control parasite replication. However, after infections using the type 1
454 parasite genotype we observed a significant reduction in Δ *GRA28* parasite burden in the brain
455 compared to wild type parasites. This effect was unexpected given the fact that parasite burden
456 was statistically equivalent during the acute phase of infection, but points to a potential

457 important role for GRA28 in altering the host innate immune response in a manner that
458 increases host susceptibility to dissemination of *T. gondii* across critical barriers like that
459 guarding the CNS. *T. gondii* can infect blood-brain barrier epithelial cells as a means to cross
460 into the host CNS (43), so GRA28 may promote parasite survival at this critical interface by
461 recruitment of regulatory T cells or other cell types that might downregulate inflammatory
462 responses.

463

464 **Summary:** Taken together our data point to a specific role of *T. gondii* GRA28 in modulating
465 chemokine production in the infected cell. Importantly, this effect occurs only in certain cell
466 types, including cells from both human and mouse placenta. A relatively small number of host
467 chemokines are affected by parasites expressing this gene, and it plays a role in both
468 modulation of the inflammatory response (as evidenced by mouse behavior and appearance
469 during infection) and ultimately parasite dissemination to “privileged” sites like the CNS.

470

471 **METHODS**

472 **Cell Culture**

473 All cell and tissue cultures were incubated at 37°C and 5% CO₂. All media were supplemented
474 with 10% fetal bovine serum (FBS; Atlas Biologicals), 2 mM L-glutamine, and 50 mg/mL
475 penicillin-streptomycin. Human foreskin fibroblast (HFF) cells were grown in Dulbecco's
476 Modified Eagle Medium (DMEM; Gibco), Raw264.7 cells were grown in DMEM (Gibco) with 10
477 mM HEPES, and THP-1 cells were grown in RPMI 1640 medium (Corning). THP-1 cells were
478 assayed for viability using Trypan Blue staining (0.4%) (Gibco), counted, spun at 120 x g for 10
479 minutes at 24°C and medium replaced with supplemented DMEM prior to infection. All THP-1
480 cell numbers listed are based on trypan blue-negative cells.

481 **Human Placental Explants**

482 Human placental tissue from less than 24 weeks of gestation was obtained, cultured, and
483 infected with *T. gondii* as described previously (44).

484 **Mouse Placental Explants**

485 Mouse placental tissues were obtained by dissection of E12.5 or 18.5 Swiss Webster mice.
486 Upon removing the fetuses from the mother, the placentas were dissected away from other
487 tissues and placed into pre-warmed 37°C PBS. The placentas were washed 3x in fresh pre-
488 warmed PBS. Each placenta was then cut in half with sterilized surgical scissors and each half
489 was placed into a well on a plate with pre-warmed 37°C DMEM with 10 mM HEPES, 10% FBS ,
490 2 mM L-glutamine, and 50 mg/mL penicillin-streptomycin. Each placenta had one half-piece of
491 tissue represented in each treatment group. For *T. gondii* infections, isolated tissue was infected
492 immediately with 5.0×10^5 – 2.0×10^6 parasites for ~24 hours.

493 **Parasites**

494 Type 1 (RH, GT1), Type 2 (Me49, Pru), Type 3 (Veg, CEP) *Toxoplasma gondii* tachyzoites and
495 sporozoites, *Neospora caninum* (NC-1) tachyzoites, and *Hammondia hammondi* (HhCatAmer
496 and HhCatEth1; (45, 46)) sporozoites were used in this study. Sporozoites were excysted from
497 sporulated oocysts as described (47) and either used immediately or grown for 24 h in human
498 foreskin fibroblasts prior to being used in controlled infections. Tachyzoites were maintained by
499 continual passage in human foreskin fibroblast (HFF) cultures incubated at 37°C and 5% CO₂ in
500 DMEM supplemented with 10% fetal bovine serum (FBS) (Atlas Biologicals), 2 mM L-glutamine,
501 and 50 mg/mL penicillin-streptomycin. The Rh *YFP* strain was a gift from David Roos (University
502 of Pennsylvania), the Rh Δ *MYR1* and Rh Δ *MYR1:MYR1_c* parasites (13) were a gift from John
503 Boothroyd (Stanford University), the PRU Δ GRA18 and complemented knockout parasites were
504 shared by Alexandre Bougdour (18), and the Pru Δ *Toxofilin* KO parasites (19) were a gift from
505 Melissa Lodoen (UC Irvine). For infections, infected monolayers were washed with fresh

506 cDMEM and then scraped and syringe lysed to release tachyzoites. These tachyzoites were
507 then passed through a 5 μ M syringe filter and counted. Parasites were then centrifuged at 800 x
508 g for 10 minutes at 24°C and resuspended and diluted in cDMEM before being used in
509 infections. Mock treatments were produced by filtering the same parasites through a 0.22 μ M
510 syringe filter and exposing host cells to the same volume of the filtrate as was used for parasite
511 infections. Freeze treatments were produced by subjecting the parasites to -80°C for 15
512 minutes, fixation treatments by exposure to 4% paraformaldehyde for 10 minutes followed by
513 washing in PBS, and sonication treatments by sonicating at 0°C using five 30-second bursts at
514 50 amps with 30-second cooling intervals in between bursts followed by microcentrifugation at
515 800 x g for 10 minutes to generate soluble (S) and pellet (P) fractions.

516 **Invasion inhibitor assays**

517 For Cytochalasin-D (Cyt-D) treatment, parasites were pre-treated with 10 μ g/mL of Cyt-D in
518 cDMEM for 1 hour and then used to infect cells in the presence of 10 μ g/mL of Cyt-D in cDMEM
519 for the duration of infection. Vehicle of Cyt-D is DMSO (40 μ L per mL of cDMEM). For 4-
520 Bromophenacyl bromide (4-BPB) treatment, parasites were pre-treated with either 0.5 or 1 μ M
521 of 4-BPB for 15 minutes. 4-BPB was dissolved directly in cDMEM. Parasites were then washed
522 twice with normal cDMEM with 10-minute 800 x g spin steps between each wash, and then
523 used to infect cells in the presence of normal cDMEM.

524 **Plaque Assays**

525 Parasites were serially diluted in media and used to infect monolayers so that each tissue
526 culture flask of HFFs received 100 parasites. These flasks were then incubated at 37°C in 5%
527 CO₂ undisturbed for 5-7 days. At the end of the incubation period, each flask was counted for
528 number of plaques present and parasite viability was calculated. Crystal violet staining was
529 used to count plaques as follows: the monolayer was washed with PBS and fixed for 5 minutes
530 with ethanol. Then crystal violet solution (12.5 g crystal violet in 125 mL ethanol mixed with 500

531 mL 1% ammonium oxalate in water) was introduced to the monolayer and allowed to stain for 5
532 minutes. The monolayer was then washed extensively with PBS and allowed to air dry prior to
533 counting plaques.

534 **Candidate gene identification using transcript level correlation analysis**

535 To identify candidate effectors for inducing CCL22 we exploited the fact that the CCL22
536 induction response in THP-1 and placental cells required the presence of the *T. gondii* effector
537 translocation protein MYR1 (13, 14). We hypothesized that MYR1-dependent effectors would
538 have similar transcript abundance profiles across diverse expression datasets. We downloaded
539 396 publicly available *T. gondii* microarray expression datasets from the Gene Expression
540 Omnibus platform hosted by the NCBI (48). We loaded and processed each CEL file using the
541 “affy” module implemented in R (49). Data were processed and normalized using the following
542 commands: `bgcorrect.method = "rma"`, `normalize.method = "quantiles"`, `pmcorrect.method =`
543 `"pmonly"`, `summary.method = "medianpolish"`. RMA-normalized data were exported, re-imported
544 into R and then transposed. An all-versus-all Pearson correlation matrix was generated using
545 the “cor” function from the R:Stats base module. Probe names on the Affymetrix array (in the
546 format of XX.mXXXXXX) were converted to current TGME49 gene models using data
547 downloaded from ToxoDB and the Vlookup function in Microsoft Excel. In some cases the
548 microarray annotations could not be matched to current TGME49 gene model names and are
549 shown as blanks in plots. This correlation matrix, the normalized array data used to generate it,
550 and a key to convert Affymetrix probe names current gene model names are all available on
551 Figshare (10.6084/m9.figshare.16451832). To analyze this correlation matrix we used
552 hierarchical clustering tools implemented in R including heatmap.2 (from the gplots package)
553 and the dendextend package. To identify candidate genes using this matrix we calculated the
554 mean correlations between 5 bait genes and all other queried genes from the microarray. The
555 bait genes were known to encode either components of the MYR complex themselves or known

556 TgMYR substrates (TgMYR1; (13), TgMYR2, TgMYR3 (14), TgGRA24 (16) and TgIST (15)).
557 Most of the candidate CCL22-inducing genes were identified based on having a) an average
558 correlation with the 5 “bait” genes listed above ≥ 0.7 , b) a dN/dS ratio ≥ 2 , c) and the presence of
559 a predicted signal peptide OR at least one transmembrane domain (which we reasoned could
560 be a cryptic signal peptide if the wrong start codon was chosen for the current gene annotation).

561 **De novo transcript assembly**

562 To identify and assemble transcripts coding for GRA28 we used *de novo* transcript assembler
563 Trinity ((50); version 2.6.6; default settings) using triplicate RNAseq datasets from WT *T. gondii*
564 RH parasites infecting THP-1 cells (see below). Assembled transcripts with similarity to the
565 predicted *GRA28* gene (TGME49_231960) were identified using BLASTN and BLASTX.
566 Primary plots were generated using GenePalette software (51) and then modified.

567 **CRISPR-mediated gene disruption and validation of knockouts**

568 The pSAG1::CAS9-U6::sgUPRT plasmid provided David Sibley (Addgene plasmid #54467;(52))
569 was modified using the Q5 Site-Directed Mutagenesis Kit (NEB) so that the gRNA sequence
570 was replaced with two restriction enzyme sites (sequence: GTTTAAACGGCCGGCC) for PseI
571 (NEB R0560S) and FseI (NEB R0588S). This modified plasmid was then used as the template
572 for all future Q5 reactions. Two unique gRNA sequences were created for each candidate gene
573 by utilizing the genomic sequences for *T. gondii* GT1 (toxodb.org) and E-CRISP (e-crisp.org)
574 using the ToxoDB-7.1.31 reference genome. A forward primer for each gRNA was created for
575 use with the modified pSAG plasmid, with the unique gRNA sequence followed by a section of
576 the plasmid scaffolding (GTTTTAGAGCTAGAAATAGCAAG). The reverse primer used with this
577 plasmid is AACTTGACATCCCCATTTAC. The gRNA sequences for the genes mentioned in this
578 study and the primers used to validate the knockouts are listed in **Supplementary Table 1**.

579 A plasmid was created for each gene of interest (GOI) using the modified pSAG plasmid
580 template and the Q5 Site-Directed Mutagenesis Kit (NEB) by following the manufacturer’s

581 protocol with a few adaptations. The KLD enzyme step was extended to 60 minutes incubation
582 at room temperature, and following the KLD enzyme step the product was heated to 65°C for 20
583 minutes and then double digested with PseI and FseI in CutSmart buffer (NEB) for 60 minutes
584 at 37°C to remove any remaining plasmid that was not eliminated by the DpnI in the KLD step.
585 This digested product was then heated to 65°C for 20 minutes to deactivate the enzymes prior
586 to transformation, plasmid isolation and sequencing to validate insertion of the correct gRNA
587 sequence (pSAG:GOI:gRNA). Parasites were transfected with either a single gRNA plasmid or
588 equal amounts of plasmids encoding two gRNAs targeting the same gene. For validation of
589 knockouts after cloning, a clone was considered a knockout if PCR across a targeted cut site
590 failed or if a PCR reaction across the entire gene (just upstream and downstream of the start
591 and stop codons, respectively) failed. In some cases where all PCR reactions worked (indicating
592 that the plasmid failed to insert at the gRNA target site), the amplified band was sequenced and
593 a clone was considered a knockout if insertions/deletions were identified near the gRNA binding
594 that resulted in frame shifts and premature stop codons.

595 **Parasite transfections**

596 In general, transfections were performed using standard approaches. Briefly, parasite
597 suspensions were obtained by needle passage (25 and 27 gauge needles) and then pelleted for
598 10 minutes at 800 x g. Parasites ($\sim 2 \times 10^7$ per transfection) were re-suspended in Cytomix (120
599 mM KCl; 0.15 mM CaCl₂; 10 mM KPO₄; 25 mM HEPES, 2mM EDTA, 5mM MgCl₂; pH to 7.6)
600 containing GSH and ATP and electroporated at 1.6 Kv with a capacitance setting of 25 μ F using
601 a BTX ECM600 Electroporator. Transfected parasites were then used to infect coverslips and/or
602 flasks of confluent HFFs and placed under appropriate selection. For candidate gene knockouts,
603 $\sim 2 \times 10^7$ *T. gondii* RH Δ HPT parasites were transfected with ~ 30 -50 μ g of the relevant
604 pSAG:GOI:gRNA plasmid(s) (described above) along with 2-5 μ g of an empty pGRA-HA-HPT
605 (53) plasmid. Parasites were placed under selection the next day and cloned by limiting dilution

606 after 2-3 passages. Individual clones were screened for gene deletion by PCR and sequencing
607 to permit identification of both target gene disruptions (via insertion of the pGRA-HA-HPT
608 plasmid at the CAS9 cut site) or mutation via DNA repair events at the CAS9 cut site. For HA-
609 tagging experiments, Type 1 (RH) *GRA28* exon 1 (residues 1-498) was C-terminally HA tagged
610 by cloning into the *T. gondii* expression plasmid pGRA-HA-HPT (53). This plasmid drives
611 protein expression using the highly active *GRA1* promoter. TgRH Δ HPT or *N. caninum* Liverpool
612 (NcLIV Δ HPT; (54)) parasites were transfected with ~40-60 μ g of *GRA28* exon 1 plasmid and
613 cells were grown overnight in normal media. For analysis of transiently transfected parasites,
614 cells were only grown for 18 h post-transfection while for stable transfection parasites were
615 grown for 2-3 passages in media containing 50 μ g/mL of mycophenolic acid and xanthine. Cells
616 were fixed with 4% PFA and permeabilized in 0.1%Triton/PBS. Samples were probed with anti-
617 HA rat monoclonal antibody (3F10 clone, Roche) diluted to 0.1 mg/mL in 0.1%Triton-PBS buffer
618 and washed four times in PBS. Samples were then incubated in 488 goat anti-rat (Life
619 Technologies Alexa Fluor H+L) followed by PBS washes. All samples were mounted in
620 Vectashield with DAPI (Vector laboratories). For genetic complementation, TgRH Δ GRA28
621 parasites were transfected the exon 1 construct used above or a construct amplified from
622 genomic DNA encompassing the start and stop codons of the GT1 version of *GRA28*
623 (TGGT1_231960). Expression plasmids (~30 μ g) were co-transfected along ~5 μ g of
624 pLIC_3xHA_DHFR* plasmid (kindly provided by Vern Carruthers; (55)), and populations were
625 placed under 1 μ M pyrimethamine selection for 2-3 weeks, and then used to infect THP-1 cells
626 for 24 h as above followed by assays to quantify CCL22 in culture supernatants by ELISA.

627

628 **Fluorescence image analysis**

629 To compare signal intensity in the nucleus of host cells infected with either *T. gondii* or *N.*
630 *caninum* parasites transiently transfected with the HA-tagged *GRA28* exon 1 construct, we
631 scanned stained coverslips for *GRA28*-HA-positive vacuoles, and then used Fiji (an

632 implementation of Imagej;) to calculate 1) the average HA signal intensity in the nucleus of the
633 infected host cell (*AvgIntInf*), 2) the average HA signal intensity in the nucleus of a neighboring,
634 uninfected host cell (*AvgIntUninf*) and 3) the average signal intensity of the parasite-containing
635 vacuole (*AvgIntVacuole*). We then used the following calculation to determine the normalized,
636 background-subtracted nuclear signaling intensity:

$$\frac{(AvgIntInf - AvgIntUninf)}{AvgIntVacuole}$$

637 Example images of this process are shown in **Figure 5** and **Figure 5 Supplement 1**. Data were
638 log₁₀ transformed prior to performing a Student's T-test.

639 **RNA-seq**

640 RNA was isolated from cultures using the RNeasy Mini Kit (QIAGEN) and its associated RNase-
641 Free DNase digestion set (QIAGEN), following the manufacturer's protocol for mammalian cells.
642 An Agilent Bioanalyzer was used to check the quality of the RNA samples. Tru-Seq stranded
643 mRNA libraries were generated from 5-17 ng/μl of mRNA for THP-1 cells, and 50-120 ng/μL of
644 mRNA for murine PECs and placental explants, and sequenced with an Illumina NextSeq 500
645 sequencer. mRNA-Seq FASTQ reads were mapped to the human reference genome (Homo
646 sapiens v81; hg38) using default options on CLC Genomics Workbench 11 (Qiagen). Total gene
647 reads (with at least 1 read count) were exported from CLC Genomics Workbench and used for
648 DESeq2 (56) to perform differential expression analysis using methods outlined previously (e.g.,
649 (4)). Data were evaluated using principal component analysis (embedded in the DESeq2
650 package) and genes were deemed to be significantly expressed if the log₂ fold-change was ≥ 1
651 or ≤ -1 and with a P_{adj} value <0.01. Gene set enrichment analysis (GSEA;(57)) and Ingenuity
652 Pathway Analysis (QIAGEN; (58)) software were used to compare gene sets that were
653 differentially regulated after infection with WT and Δ*GRA28* parasites.

654 **CCL22 and Ccl22 ELISA**

655 CCL22/Ccl22 ELISAs were performed on culture supernatants (undiluted or diluted when
656 necessary) using Immulon 4HBX flat bottom microtiter plates with the human CCL22/MDC
657 DuoSet ELISA (R&D Systems DY336) or the mouse Ccl22/Mdc DuoSet ELISA (R&D Systems
658 DY439) per the manufacturer's instructions.

659 **Mouse Experiments with WT and Δ GRA28 parasites**

660 To determine the impact of *T. gondii* candidate effectors on mouse morbidity and cytokine
661 production, BALB/cJ mice from Jackson laboratories (4-6 week old, female) were injected
662 intraperitoneally with 200 μ L of PBS containing 1.0×10^6 *T. gondii* tachyzoites, or 200 μ L of 0.22
663 μ M filtered parasite solution as a mock treatment. Mice were sacrificed at 48 hours post
664 infection (HPI), and peritoneal exudate cells (PECs) were collected by injecting 3 mL sterile PBS
665 into the abdominal cavity, rocking the mouse to mix the PBS, and siphoning the PBS solution
666 into a sterile conical tube. The solution was then centrifuged at 1,000 x g for 10 minutes at 24°C,
667 the supernatant was collected, and RNA was extracted from the pellet for RT-qPCR and RNA-
668 seq. Blood was collected in Sarstedt Microvette CB 300 Z tubes by cardiac puncture and
669 centrifuged at 10,000 x g for 5 minutes to separate the serum. Mice were infected with RH Δ HPT
670 (wild type), RH Δ MYR1 or RH Δ GRA28 parasites depending on the experiment.

671 To determine the impact of *GRA28* deletion on *T. gondii* proliferation and dissemination,
672 female BALB/cJ mice (4 weeks old) from Jackson laboratories were injected intraperitoneally
673 with 200 μ L PBS containing 100 *T. gondii* tachyzoites. In one experiment five mice received an
674 injection of RH Δ GRA28 parasites, while the other five received an injection of the transfection
675 control parasite that was transfected with empty vector (Rh Δ HPT:HPT). For behavioral indices
676 of inflammatory responses, photographs of the mice were taken dorsally and laterally every 4-6
677 hours for the entire duration of the infection. Mice were visually scored 0-3 based on the
678 presence of fur ruffling, the location of ruffling, and the presence of skin redness/irritation

679 **(Figure 7 Supplement 1). 0)** No fur ruffling or red/irritated skin present. **1)** Mild ruffling present
680 predominantly located on the head and back of the neck. No red/irritated skin visible. **2)**
681 Moderate ruffling present - fur forms larger clumps and extends to the rest of the body. Skin
682 may be visible through the clumps but is not red or irritated. **3)** Severe ruffling characterized by
683 fur ruffling across the entire body with visibly red/irritated skin in between fur clumps.

684 In a second experiment mice were infected with 1000 tachyzoites of *T. gondii* strain
685 ME49:*LUCΔGRA28* or a passage-matched wild type strain (27, 28). Mice were imaged daily
686 after injection of D-Luciferin as described previously (28, 59) using an IVIS Lumina II *in vivo*
687 bioluminescence imaging system (with ventral imaging occurring on all days post-infection and
688 ventral and dorsal imaging occurring starting on day 10 post-infection). Animals were
689 anaesthetized using 2% isoflurane during the 4-8 minute imaging period (ventrally and dorsally
690 where applicable). When necessary, blood was collected via submandibular lancet puncture,
691 collected into Sarstedt Microvette CB 300 Z tubes and spun at 10,000 x g for 5 minutes to
692 separate the serum. Mice were monitored extensively over the course of infection for symptoms
693 of morbidity and humanely euthanized. All animal procedures were approved by the Division of
694 Laboratory Animal Resources and IACUC and our animal facilities are routinely inspected by
695 the USDA and local IACUC committee.

696 **Statistics**

697 All statistics were performed in Graphpad Prism for Windows (versions 7 or 9; GraphPad
698 Software, La Jolla, CA). For most two treatment assays, we used unpaired, two-tailed student's
699 T test, and for multi-treatment/condition experiments we used one- or two-way ANOVA followed
700 by multiple comparisons post-hoc tests. Individual comparisons are listed for each assay in the
701 text and figure legend, and only pre-planned comparisons were performed to minimize Type 1
702 error. *In vivo* bioluminescence data (total flux; photons/s) and nuclear staining intensity data

703 (comparing nuclear trafficking of *T. gondii* GRA28 when expressed in *T. gondii* or *N. caninum*)
704 were log₁₀-transformed prior to statistical analysis.

705 **Acknowledgements**

706 The authors would like to thank Dr. Alexandre Bougdour (Inserm; Grenoble, France) for
707 providing GRA18 knockout and complemented strains, Drs. John Boothroyd and Michael Panas
708 (Stanford University) for helpful discussions and providing MYR1 knockout and complemented
709 strains, and Dr. Peter Bradley (University of California-Los Angeles) for helpful discussions and
710 sharing reagents related to GRA28 that facilitated this work.

711 **BIBLIOGRAPHY**

- 712 1. Fallahi S, Rostami A, Nourollahpour Shiadeh M, Behniafar H, Paktinat S. 2018. An
713 updated literature review on maternal-fetal and reproductive disorders of *Toxoplasma*
714 *gondii* infection. J Gynecol Obstet Hum Reprod 47:133–140.
- 715 2. Stagno S, Reynolds DW, Amos CS, Dahle AJ, McCollister FP, Mohindra I, Ermocilla R,
716 Alford CA. 1977. Auditory and visual defects resulting from symptomatic and subclinical
717 congenital cytomegaloviral and *Toxoplasma* infections. Pediatrics 59:669–678.
- 718 3. Fahnehjelm KT, Malm G, Ygge J, Engman ML, Maly E, Evengård B. 2000.
719 Ophthalmological findings in children with congenital toxoplasmosis. Report from a
720 Swedish prospective screening study of congenital toxoplasmosis with two years of follow-
721 up. Acta Ophthalmol Scand 78:569–575.
- 722 4. Ander SE, Rudzki EN, Arora N, Sadovsky Y, Coyne CB, **Boyle JP**. 2018. Human
723 Placental Syncytiotrophoblasts Restrict *Toxoplasma gondii* Attachment and Replication
724 and Respond to Infection by Producing Immunomodulatory Chemokines. MBio 9.
- 725 5. Klarquist J, Tobin K, Farhangi Oskuei P, Henning SW, Fernandez MF, Dellacecca ER,
726 Navarro FC, Eby JM, Chatterjee S, Mehrotra S, Clark JI, Le Poole IC. 2016. Ccl22 diverts
727 T regulatory cells and controls the growth of melanoma. Cancer Res 76:6230–6240.

- 728 6. Layseca-Espinosa E, Korniotis S, Montandon R, Gras C, Bouillie M, Gonzalez-Amaro R,
729 Dy M, Zavala F. 2013. CCL22-producing CD8 α - myeloid dendritic cells mediate regulatory
730 T cell recruitment in response to G-CSF treatment. *J Immunol* 191:2266–2272.
- 731 7. Freier CP, Kuhn C, Rapp M, Endres S, Mayr D, Friese K, Anz D, Jeschke U. 2015.
732 Expression of CCL22 and infiltration by regulatory T cells are increased in the decidua of
733 human miscarriage placentas. *Am J Reprod Immunol* 74:216–227.
- 734 8. Martinez de la Torre Y, Buracchi C, Borroni EM, Dupor J, Bonecchi R, Nebuloni M,
735 Pasqualini F, Doni A, Lauri E, Agostinis C, Bulla R, Cook DN, Haribabu B, Meroni P,
736 Rukavina D, Vago L, Tedesco F, Vecchi A, Lira SA, Locati M, Mantovani A. 2007.
737 Protection against inflammation- and autoantibody-caused fetal loss by the chemokine
738 decoy receptor D6. *Proc Natl Acad Sci USA* 104:2319–2324.
- 739 9. Martinenaitė E, Munir Ahmad S, Hansen M, Met Ö, Westergaard MW, Larsen SK,
740 Klausen TW, Donia M, Svane IM, Andersen MH. 2016. CCL22-specific T Cells:
741 Modulating the immunosuppressive tumor microenvironment. *Oncoimmunology*
742 5:e1238541.
- 743 10. Kimura S, Tanimoto A, Wang K-Y, Shimajiri S, Guo X, Tasaki T, Yamada S, Sasaguri Y.
744 2012. Expression of macrophage-derived chemokine (CCL22) in atherosclerosis and
745 regulation by histamine via the H2 receptor. *Pathol Int* 62:675–683.
- 746 11. Rynning FW, Remington JS. 1978. Effect of cytochalasin D on *Toxoplasma gondii* cell
747 entry. *Infect Immun* 20:739–743.
- 748 12. Li L, Li X, Yan J. 2008. Alterations of concentrations of calcium and arachidonic acid and
749 agglutinations of microfilaments in host cells during *Toxoplasma gondii* invasion. *Vet*
750 *Parasitol* 157:21–33.
- 751 13. Franco M, Panas MW, Marino ND, Lee M-CW, Buchholz KR, Kelly FD, Bednarski JJ,
752 Sleckman BP, Pourmand N, Boothroyd JC. 2016. A novel secreted protein, MYR1, is
753 central to *Toxoplasma*'s manipulation of host cells. *MBio* 7:e02231–15.

- 754 14. Marino ND, Panas MW, Franco M, Theisen TC, Naor A, Rastogi S, Buchholz KR, Lorenzi
755 HA, Boothroyd JC. 2018. Identification of a novel protein complex essential for effector
756 translocation across the parasitophorous vacuole membrane of *Toxoplasma gondii*. PLoS
757 Pathog 14:e1006828.
- 758 15. Olias P, Etheridge RD, Zhang Y, Holtzman MJ, Sibley LD. 2016. *Toxoplasma* Effector
759 Recruits the Mi-2/NuRD Complex to Repress STAT1 Transcription and Block IFN- γ -
760 Dependent Gene Expression. Cell Host Microbe 20:72–82.
- 761 16. Braun L, Brenier-Pinchart M-P, Yogavel M, Curt-Varesano A, Curt-Bertini R-L, Hussain T,
762 Kieffer-Jaquinod S, Coute Y, Pelloux H, Tardieux I, Sharma A, Belrhali H, Bougdour A,
763 Hakimi M-A. 2013. A *Toxoplasma* dense granule protein, GRA24, modulates the early
764 immune response to infection by promoting a direct and sustained host p38 MAPK
765 activation. J Exp Med 210:2071–2086.
- 766 17. Shastri AJ, Marino ND, Franco M, Lodoen MB, Boothroyd JC. 2014. GRA25 is a novel
767 virulence factor of *Toxoplasma gondii* and influences the host immune response. Infect
768 Immun 82:2595–2605.
- 769 18. He H, Brenier-Pinchart M-P, Braun L, Kraut A, Touquet B, Couté Y, Tardieux I, Hakimi M-
770 A, Bougdour A. 2018. Characterization of a *Toxoplasma* effector uncovers an alternative
771 GSK3/ β -catenin-regulatory pathway of inflammation. Elife 7.
- 772 19. Lodoen MB, Gerke C, Boothroyd JC. 2010. A highly sensitive FRET-based approach
773 reveals secretion of the actin-binding protein toxofilin during *Toxoplasma gondii* infection.
774 Cell Microbiol 12:55–66.
- 775 20. Delorme-Walker V, Abrivard M, Lagal V, Anderson K, Perazzi A, Gonzalez V, Page C,
776 Chauvet J, Ochoa W, Volkmann N, Hanein D, Tardieux I. 2012. Toxofilin upregulates the
777 host cortical actin cytoskeleton dynamics, facilitating *Toxoplasma* invasion. J Cell Sci
778 125:4333–4342.

- 779 21. Riezu-Boj J-I, Larrea E, Aldabe R, Guembe L, Casares N, Galeano E, Echeverria I,
780 Sarobe P, Herrero I, Sangro B, Prieto J, Lasarte J-J. 2011. Hepatitis C virus induces the
781 expression of CCL17 and CCL22 chemokines that attract regulatory T cells to the site of
782 infection. *J Hepatol* 54:422–431.
- 783 22. Jeong S-I, Choi B-M, Jang SI. 2010. Sulforaphane suppresses TARC/CCL17 and
784 MDC/CCL22 expression through heme oxygenase-1 and NF- κ B in human keratinocytes.
785 *Arch Pharm Res* 33:1867–1876.
- 786 23. Wiley M, Teygong C, Phelps E, Radke J, Blader IJ. 2011. Serum response factor
787 regulates immediate early host gene expression in *Toxoplasma gondii*-infected host cells.
788 *PLoS One* 6:e18335.
- 789 24. Saeij JPJ, Collier S, **Boyle JP**, Jerome ME, White MW, Boothroyd JC. 2007. *Toxoplasma*
790 co-opts host gene expression by injection of a polymorphic kinase homologue. *Nature*
791 445:324–327.
- 792 25. Nadipuram SM, Kim EW, Vashisht AA, Lin AH, Bell HN, Coppens I, Wohlschlegel JA,
793 Bradley PJ. 2016. *In vivo* biotinylation of the *Toxoplasma* parasitophorous vacuole reveals
794 novel dense granule proteins important for parasite growth and pathogenesis. *MBio* 7.
- 795 26. English ED, Adomako-Ankomah Y, **Boyle JP**. 2015. Secreted effectors in *Toxoplasma*
796 *gondii* and related species: determinants of host range and pathogenesis? *Parasite*
797 *Immunol* 37:127–140.
- 798 27. Blank ML, Parker ML, Ramaswamy R, Powell CJ, English ED, Adomako-Ankomah Y,
799 Pernas LF, Workman SD, Boothroyd JC, Boulanger MJ, **Boyle JP**. 2018. A *Toxoplasma*
800 *gondii* locus required for the direct manipulation of host mitochondria has maintained
801 multiple ancestral functions. *Mol Microbiol* 108:519–535.
- 802 28. English ED, **Boyle JP**. 2018. Impact of Engineered Expression of Mitochondrial
803 Association Factor 1b on *Toxoplasma gondii* Infection and the Host Response in a Mouse
804 Model. *mSphere* 3.

- 805 29. Hakimi M-A, Olias P, Sibley LD. 2017. *Toxoplasma* effectors targeting host signaling and
806 transcription. Clin Microbiol Rev 30:615–645.
- 807 30. Lee CW, Sukhumavasi W, Denkers EY. 2007. Phosphoinositide-3-kinase-dependent,
808 MyD88-independent induction of CC-type chemokines characterizes the macrophage
809 response to *Toxoplasma gondii* strains with high virulence. Infect Immun 75:5788–5797.
- 810 31. Hill RD, Gouffon JS, Saxton AM, Su C. 2012. Differential gene expression in mice infected
811 with distinct *Toxoplasma* strains. Infect Immun 80:968–974.
- 812 32. Jensen KDC, Wang Y, Wojno EDT, Shastri AJ, Hu K, Cornel L, Boedec E, Ong Y-C,
813 Chien Y, Hunter CA, Boothroyd JC, Saeij JPJ. 2011. *Toxoplasma* polymorphic effectors
814 determine macrophage polarization and intestinal inflammation. Cell Host Microbe 9:472–
815 483.
- 816 33. Rosowski EE, Lu D, Julien L, Rodda L, Gaiser RA, Jensen KDC, Saeij JPJ. 2011. Strain-
817 specific activation of the NF-kappaB pathway by GRA15, a novel *Toxoplasma gondii*
818 dense granule protein. J Exp Med 208:195–212.
- 819 34. Lee JW, Zemojtel T, Shakhnovich E. 2009. Systems-level evidence of transcriptional co-
820 regulation of yeast protein complexes. J Comput Biol 16:331–339.
- 821 35. Rosenberg A, Sibley LD. 2021. *Toxoplasma gondii* secreted effectors co-opt host
822 repressor complexes to inhibit necroptosis. Cell Host Microbe.
- 823 36. Ong Y-C, Reese ML, Boothroyd JC. 2010. *Toxoplasma* rhoptry protein 16 (ROP16)
824 subverts host function by direct tyrosine phosphorylation of STAT6. J Biol Chem
825 285:28731–28740.
- 826 37. Gay G, Braun L, Brenier-Pinchart M-P, Vollaire J, Josserand V, Bertini R-L, Varesano A,
827 Touquet B, De Bock P-J, Coute Y, Tardieux I, Bougdour A, Hakimi M-A. 2016.
828 *Toxoplasma gondii* TglST co-opts host chromatin repressors dampening STAT1-
829 dependent gene regulation and IFN- γ -mediated host defenses. J Exp Med 213:1779–
830 1798.

- 831 38. Gupta D, Wang Q, Vinson C, Dziarski R. 1999. Bacterial peptidoglycan induces CD14-
832 dependent activation of transcription factors CREB/ATF and AP-1. J Biol Chem
833 274:14012–14020.
- 834 39. Hall AJ, Vos HL, Bertina RM. 1999. Lipopolysaccharide induction of tissue factor in THP-1
835 cells involves Jun protein phosphorylation and nuclear factor kappaB nuclear
836 translocation. J Biol Chem 274:376–383.
- 837 40. Wan J, Shan Y, Fan Y, Fan C, Chen S, Sun J, Zhu L, Qin L, Yu M, Lin Z. 2016. NF-κB
838 inhibition attenuates LPS-induced TLR4 activation in monocyte cells. Mol Med Rep
839 14:4505–4510.
- 840 41. Carruthers VB, Håkansson S, Giddings OK, Sibley LD. 2000. *Toxoplasma gondii* uses
841 sulfated proteoglycans for substrate and host cell attachment. Infect Immun 68:4005–
842 4011.
- 843 42. Harper JM, Hoff EF, Carruthers VB. 2004. Multimerization of the *Toxoplasma gondii* MIC2
844 integrin-like A-domain is required for binding to heparin and human cells. Mol Biochem
845 Parasitol 134:201–212.
- 846 43. Konradt C, Ueno N, Christian DA, DeLong JH, Pritchard GH, Herz J, Bzik DJ, Koshy AA,
847 McGavern DB, Lodoen MB, Hunter CA. 2016. Endothelial cells are a replicative niche for
848 entry of *Toxoplasma gondii* to the central nervous system. Nat Microbiol 1:16001.
- 849 44. Platt DJ, Smith AM, Arora N, Diamond MS, Coyne CB, Miner JJ. 2018. Zika virus-related
850 neurotropic flaviviruses infect human placental explants and cause fetal demise in mice.
851 Sci Transl Med 10.
- 852 45. Dubey JP, Tilahun G, **Boyle JP**, Schares G, Verma SK, Ferreira LR, Oliveira S, Tiao N,
853 Darrington C, Gebreyes WA. 2013. Molecular and biological characterization of first
854 isolates of *Hammondia hammondi* from cats from Ethiopia. J Parasitol 99:614–618.
- 855 46. Dubey JP, Sreekumar C. 2003. Redescription of *Hammondia hammondi* and its
856 differentiation from *Toxoplasma gondii*. Int J Parasitol 33:1437–1453.

- 857 47. Sokol SL, Primack AS, Nair SC, Wong ZS, Tembo M, Verma SK, Cerqueira-Cezar CK,
858 Dubey JP, **Boyle JP**. 2018. Dissection of the *in vitro* developmental program of
859 *Hammondia hammondi* reveals a link between stress sensitivity and life cycle flexibility in
860 *Toxoplasma gondii*. *Elife* 7.
- 861 48. Barrett T, Wilhite SE, Ledoux P, Evangelista C, Kim IF, Tomashevsky M, Marshall KA,
862 Phillippy KH, Sherman PM, Holko M, Yefanov A, Lee H, Zhang N, Robertson CL, Serova
863 N, Davis S, Soboleva A. 2013. NCBI GEO: archive for functional genomics data sets--
864 update. *Nucleic Acids Res* 41:D991–5.
- 865 49. Gautier L, Cope L, Bolstad BM, Irizarry RA. 2004. affy--analysis of Affymetrix GeneChip
866 data at the probe level. *Bioinformatics* 20:307–315.
- 867 50. Grabherr MG, Haas BJ, Yassour M, Levin JZ, Thompson DA, Amit I, Adiconis X, Fan L,
868 Raychowdhury R, Zeng Q, Chen Z, Mauceli E, Hacohen N, Gnirke A, Rhind N, di Palma
869 F, Birren BW, Nusbaum C, Lindblad-Toh K, Friedman N, Regev A. 2011. Full-length
870 transcriptome assembly from RNA-Seq data without a reference genome. *Nat Biotechnol*
871 29:644–652.
- 872 51. Smith AF, Posakony JW, Rebeiz M. 2017. Automated tools for comparative sequence
873 analysis of genic regions using the GenePalette application. *Dev Biol* 429:158–164.
- 874 52. Shen B, Brown KM, Lee TD, Sibley LD. 2014. Efficient gene disruption in diverse strains
875 of *Toxoplasma gondii* using CRISPR/CAS9. *MBio* 5:e01114–14.
- 876 53. Saeij JPJ, **Boyle JP**, Coller S, Taylor S, Sibley LD, Brooke-Powell ET, Ajioka JW,
877 Boothroyd JC. 2006. Polymorphic secreted kinases are key virulence factors in
878 toxoplasmosis. *Science* 314:1780–1783.
- 879 54. Coombs RS, Blank ML, English ED, Adomako-Ankomah Y, Urama I-CS, Martin AT,
880 Yarovinsky F, **Boyle JP**. 2020. Immediate Interferon Gamma Induction Determines
881 Murine Host Compatibility Differences between *Toxoplasma gondii* and *Neospora*
882 *caninum*. *Infect Immun* 88.

- 883 55. Huynh M-H, Carruthers VB. 2009. Tagging of endogenous genes in a *Toxoplasma gondii*
884 strain lacking Ku80. *Eukaryotic Cell* 8:530–539.
- 885 56. Love MI, Huber W, Anders S. 2014. Moderated estimation of fold change and ' ' dispersion
886 for RNA-seq data with DESeq2. *Genome Biol* 15:550.
- 887 57. Croken MM, Qiu W, White MW, Kim K. 2014. Gene Set Enrichment Analysis (GSEA) of
888 *Toxoplasma gondii* expression datasets links cell cycle progression and the bradyzoite
889 developmental program. *BMC Genomics* 15:515.
- 890 58. Krämer A, Green J, Pollard J, Tugendreich S. 2014. Causal analysis approaches in
891 Ingenuity Pathway Analysis. *Bioinformatics* 30:523–530.
- 892 59. Saeij JPJ, **Boyle JP**, Grigg ME, Arrizabalaga G, Boothroyd JC. 2005. Bioluminescence
893 imaging of *Toxoplasma gondii* infection in living mice reveals dramatic differences
894 between strains. *Infect Immun* 73:695–702.
- 895
- 896

897 **FIGURE LEGENDS:**

898

899 **Figure 1:** A) THP-1 cells, Human Foreskin Fibroblasts (HFFs), and 2nd trimester placental
900 samples of villous trees and decidual tissue were infected with a type I strain of *Toxoplasma*
901 *gondii* (RH:YFP). Statistics on the THP-1 cell and HFF cell samples performed by ordinary Two-
902 way ANOVA analysis with Tukey's multiple comparisons test. Statistics on the placental
903 samples performed by two-tailed welch-corrected t-tests. B) Type I strain (RH) *T. gondii*
904 parasites subjected to multiple treatments as described in methods. The soluble fraction of the
905 sonicated treatment is denoted by S, the insoluble fraction is denoted by P. THP-1 cells were
906 then exposed to either live parasites, or treated parasites. Statistics performed by multiple two-
907 tailed welch-corrected t-test comparisons with the live parasite treatment $P \leq 0.0145$. C,D) Type
908 I strain (RH) *T. gondii* parasites were treated with either Cytochalasin D (C), or 4-
909 Bromophenacyl bromide (D) as described in methods. THP-1 cells were then infected with the
910 respective parasite treatment. Statistics were performed by two-way ANOVA analysis and
911 multiple comparisons post-hoc tests, where Cyt-D $P = 0.009$, and 4-BPB $P < 0.0001$. E) Type I
912 strain (RH) *T. gondii* parasites deficient in Myr-1 (TgRHΔMyr-1) and their complement
913 (TgRHΔMyr-1:Myr-1_{comp}) were used to infect THP-1 cells. (F) Type I strain (RH) *T. gondii*
914 parasites were used to infect THP-1 cells at MOIs of: 20, 10, 8, 6, 4, 3, 1, 0.8, 0.4, 0.2, and 0.1.
915 A, B, C, D) Respective cells/tissues were infected with a multiplicity of infection (MOI) of 3.
916 Supernatants were collected at 24 hours post-infection unless indicated otherwise, and assayed
917 by CCL22 ELISA.

918

919 **Figure 2:** Transcript correlation analyses to identify putative MYR1 substrates based on 396
920 publicly available microarray datasets. A) Gene-by-gene correlation data for *T. gondii* genes
921 across 396 microarray datasets. A subset (3,217 genes with at least one sample having a
922 normalized log2-transformed value ≥ 10) of the total number (8,058) of *T. gondii* genes are

923 shown for simplicity. Genes outlined in the green box indicate the cluster containing all of the
924 bait genes as well as candidate CCL22-inducing genes with the exception of *Toxofilin*. Dark
925 blue tick marks on each dendrogram indicate the location of all of the bait genes. Color scale
926 covers correlations ranging from -1 to +1. B) Subcluster containing *MYR2* and *GRA28*. C)
927 Subcluster containing *MYR1*, *TgIST*, *GRA18* and *GRA24*. Note: For B and C the color scale is
928 from 0.5 to 1.0 to highlight subcluster differences.

929

930 **Figure 3:** Identification of the *T. gondii* gene *GRA28* as an inducer of CCL22 in human cells. A)
931 Gene expression correlations across 396 *T. gondii* expression microarrays between TgMYR1
932 and 4 additional “bait” genes (top) and 5 candidate CCL22-inducing effectors (bottom). dN/dS
933 ratios are also shown to illustrate the high level of positive selection acting on this class of
934 genes. B) Effect of deleting 5 candidate genes on CCL22 secretion in THP-1 cells, showing that
935 Δ *GRA28* parasites induced significantly less CCL22 compared to wild type controls (>100 fold
936 reduction; ***P<0.0001). PRU Δ *Toxofilin* parasites also induced significantly lower levels of
937 CCL22 in THP-1 cells (1.4-fold reduction; **P<0.01). Each blue dot indicates a genetically
938 distinct knockout clone. C) Δ *GRA28* parasite clones also induce significantly less CCL22 from
939 primary human 2nd trimester placental villous explants. D) MA plot of RNAseq analysis
940 performed on THP-1 cells infected with WT or Δ *GRA28* *T. gondii* (RH strain). CCL22 and the
941 chemokines CXL1 and CXL2 were the most highly *GRA28*-dependent transcripts, while a
942 handful (64) of other genes had significantly higher transcript abundance in WT parasites
943 compared to Δ *GRA28* parasites (P_{adj}<0.001; Log₂FC>2; blue symbols). CCL17 (arrow, green
944 symbol), a chemokine that is typically co-regulated with CCL22, did not show any evidence of
945 being induced by *GRA28*.

946

947 **Figure 4.** IPA analysis on THP-1 cells infected with WT or Δ *GRA28* *T. gondii* parasites for 24h
948 showing canonical pathways that were differentially regulated (-log(P) \geq 2; Z score \leq -2 or \geq 2)

949 depending on the presence or absence of the GRA28 gene. A) Z scores for significant canonical
950 pathways. All were higher in WT compared to Δ GRA28 *T. gondii*. B) There was extensive
951 overlap of component genes within each canonical pathway, particularly for the genes *KL* and
952 those encoding components of the AP-1 transcription factor complex (*JUN* and *FOS*). A
953 heatmap of fold-difference in transcript abundance for cells infected with RH:WT and
954 RH Δ GRA28 is shown. C) GRA28 is responsible for driving transcriptional changes in two major
955 gene clusters identified based on the degree of gene sharing between each canonical pathway
956 (clusters outlined in dotted green boxes). The larger cluster consists primarily of immunity-
957 related pathways while the smaller cluster consists of genes involved in proteoglycan synthesis.
958 D) Quantification of NF κ B activation in 293T cells. Cells were transfected with NF κ B firefly
959 luciferase plasmid, a constitutive renilla luciferase plasmid, as well as empty vector (EV), a
960 construct expressing a CARD domain (dsCARDS) or the first exon of *T. gondii* GRA28. While
961 the CARD domain construct induced firefly luciferase expression as expected, expression of *T.*
962 *gondii* GRA28 had no significant impact on firefly luciferase levels (letters indicate groups that
963 were not significantly different from one another following one way ANOVA and Tukey's multiple
964 comparisons post-hoc test.)

965
966 **Figure 5:** A) Schematic of the *GRA28* locus along with its gene prediction in the current
967 annotation of the *T. gondii* genome (www.toxodb.org). In addition to gene models from two *T.*
968 *gondii* strains (GT1 and ME49), 39 bp repeats and regions used in expression constructs are
969 shown in brown and light green. Map created using GenePalette software (see Materials and
970 Methods; (51)). B) Sequence encoding an N-terminal HA tag was inserted immediately after the
971 predicted signal peptide cleavage site in a GRA1-promoter driven version of *T. gondii* GRA28
972 Exon 1. When transiently transfected into *T. gondii* HA-tagged protein could be detected in the
973 parasites as well as the host cell nucleus. C) Δ GRA28 *T. gondii* parasites (RH strain) were
974 transiently transfected with empty pGRA-HA-HPT vector (EV) or the same construct described

975 in B encoding an HA-tagged version of *T. gondii* GRA28 Exon 1. After washing in cDMEM
976 parasites were used to infect freshly plated THP-1 cells for 24h and CCL22-levels were
977 quantified in culture supernatants using ELISA. Mock-treated cells were exposed to a sterile
978 filtered parasite preparation. D) E) The construct encoding HA-tagged *T. gondii* GRA28 Exon 1
979 (same as that used in B and C) was used to transfect *Neospora caninum*, a near relative of *T.*
980 *gondii*. HA staining revealed expression of this *T. gondii* GRA28 Exon 1 in *N. caninum* parasites
981 (visualized by HA staining) but in contrast to *T. gondii* we did not observe trafficking of GRA28
982 to the host cell nucleus when expressed in this strain. Quantification of nuclear HA-derived
983 signal is presented in **Figure 5** Supplementary **Figure 1**. F) Sequences encoding an N-terminal
984 V5 tag were inserted downstream of a Kozak consensus sequence and upstream of GRA28
985 Exon 1 (minus the signal peptide-encoding sequence). The construct was transfected into HeLa
986 cells and V5 staining was observed prominently in the nucleus of transfected cells. G)
987 Transfection of the construct in E directly into RAW 264.7 cells significantly induced CCL22
988 production as detected by ELISA. T-test was performed on log₁₀-transformed data.

989

990 **Figure 6.** GRA28 induction of Ccl22 is conserved in mouse immune and placental tissues. A,B)
991 Δ GRA28 parasites induce significantly less Ccl22 secretion from RAW 264.7 macrophages (A)
992 and mouse placental explants (B) compared to wild type parasites. C) The number of host
993 genes besides Ccl22 that are GRA28-dependent in placental explants is relatively small,
994 suggesting that GRA28 is a highly specific inducer of Ccl22 in mouse placental tissue. D,E)
995 Mouse serum (D) and peritoneal lavage (E) levels of Ccl22 48 h-post-infection are dependent
996 on GRA28.

997

998 **Figure 7.** A) Mortality and B) weight loss does not significantly differ in mice infected with WT
999 and Δ GRA28 type 1 strain *T. gondii* parasites. C) Behavioral changes and fur ruffling
1000 phenotypes associated with infection are exacerbated during the acute phase of infection for

1001 mice infected with Δ GRA28 parasites compared to WT based on a phenotype scoring system.
1002 Specifically, mice infected with Δ GRA28 parasites (light grey lines and triangles) exhibited
1003 infection-related symptoms at earlier time points compared to those infected with WT parasites
1004 (black lines and circles). Curves beneath lines are the average across all mice at that time point
1005 (with lighter grey representing Δ GRA28 knockout parasites and darker grey representing wild
1006 type). *: $P < 0.05$ after Two Way ANOVA and followed by multiple comparisons at each time
1007 point.

1008

1009 **Figure 8:** Impact of the *GRA28* gene on proliferation and dissemination of Type II parasites
1010 expressing luciferase. Neither A) mortality nor B) mouse weight loss were significantly different
1011 in mice infected with WT or Δ GRA28 *T. gondii* Type II (ME49) strain parasites. C) Throughout
1012 the acute phase of infection parasite-derived bioluminescence of WT and Δ GRA28 parasites in
1013 the peritoneal cavity was measured by imaging the animals ventrally. Burden was similar
1014 ($P > 0.05$) between parasite strains at all time points except for D9 post-infection, when signal
1015 was significantly higher in Δ GRA28-infected mice compared to WT mice ($P = 0.014$). D,E)
1016 Starting on D10 post-infection we imaged mice both ventrally and dorsally to visualize
1017 dissemination to and proliferation in the mouse brain. In contrast to the acute phase we
1018 observed a consistently lower level of parasite-derived bioluminescence in the brains of mice
1019 infected with Δ GRA28 parasites compared to WT parasites on days 14 and 15 post-infection
1020 ($P = 0.016$ and 0.0002 , respectively). All statistical tests were performed on log2-transformed
1021 bioluminescent data.

1022

1023 **SUPPLEMENTAL FIGURE LEGENDS:**

1024 **Figure 1 Supplement 1:** A) Type 1 (Rh88), Type 2 (Pru) and Type 3 (CTG) *T. gondii* strains all
1025 induce CCL22 in THP-1 cells. For mock cells were treated with 0.2 micron-filtered parasite
1026 suspensions. B) *H. hammondi* induces CCL22 production in THP-1 cells while *N. caninum* does

1027 not when compared to mock-treated cells. C) The *T. gondii* gene MYR1 is required for CCL22
1028 production by THP-1 cells after infection. *T. gondii* Δ MYR1 parasites were compared to
1029 Δ MYR1:MYR1-complemented parasites and only the MYR1-complemented parasites induced
1030 secretion of CCL22 from wild type (black data points; left) or MYD88-knockout (blue data points;
1031 right) THP-1 cells. While MYD88 knockout cells produced significantly less CCL22 in response
1032 to MYR1-complemented parasites, they still produced CCL22 at levels much greater than
1033 Δ MYR1-infected cells or mock-treated cells. MYR1-knockout and complemented parasites were
1034 kindly provided by John Boothroyd and Michael Panas, Stanford University.

1035

1036 **Figure 2 Supplement 1:** Clusters of co-regulated genes share developmental expression
1037 profiles and functional activities. A) Transcript abundance correlation analysis (left) and
1038 clustered transcript abundance analysis (in RMA log₂-normalized units) for 21 genes with
1039 transcripts known to increase in abundance during the tachyzoite to bradyzoite transition,
1040 including BAG1, LDH2 and enolase. Bar across the top of the expression heatmap indicates the
1041 life cycle stage source for each of the samples. Pie chart indicates that 19 of the 21 transcripts
1042 increase in abundance during pH-induced bradyzoite development according to the Bradyzoite
1043 Differentiation (3-day Time Series) dataset on ToxoDB.org. B) Cluster containing multiple
1044 ribosomal protein coding genes (for both the large and small subunits) showing high transcript
1045 abundance in tachyzoites and bradyzoites but comparatively low transcript abundance in
1046 samples taken from sporozoites and merozoites.

1047

1048 **Figure 3 Supplementary Figure 1:** Transcript level correlation analysis with the 6 bait genes
1049 used in this study (A) and clustered, normalized gene expression data (B) for all genes in the *T.*
1050 *gondii* genome annotated with the term “dense granule” in the product name or user comments.
1051 Dense granule protein coding genes fall into two major clusters in the correlation analysis, with

1052 the top cluster containing the known secreted effectors GRA15, GRA24, TglST, GRA7 and
1053 GRA28.

1054

1055 **Figure 3 Supplementary Figure 2:** Validation of knockouts generated for the present study (A-
1056 D) of for GRA18 which was generated in another study (E; He *et al.*, eLife 2018;7:e39887).

1057 Clones that were validated as knockouts and used in the CCL22-induction assays shown in

1058 **Figure 3b** are labeled with ***bold-italic font***. We validated using two parallel approaches for most

1059 of the knockouts: (1) amplifying across the site targeted by the protospacer(s) encoded by the

1060 transfected gRNA-expressing plasmid(s) where no amplification indicated a potential insertion of

1061 plasmid sequence into that location and (2) amplifying across the entire coding sequence of the

1062 gene, where no amplification also suggests insertion of the selectable marker and other plasmid

1063 sequence at at least one of the protospacer sites. In some cases multiple protospacer encoding

1064 plasmids were transfected into the same parasite population (and protospacer numbers are our

1065 own internal nomenclature), and in these cases it was possible to have insertion/disruption at

1066 both protospacer sites (and this occurred in some instances). Primer sequences and gRNA

1067 target sites are shown in **Table S1**. A) Validation of four TGGT1_201390 knockout clones

1068 generated by batch transfection with gRNAs targeting two distinct sites in the TGGT1_201390

1069 coding sequence (2 and 12). Left gel: Two primer sets (A and B) were used to amplify across

1070 the site targeted by the protospacer, and MAF1b primers were used as a positive control.

1071 Clones D11 and G11 likely had insertions at protospacer site 2 (as evidenced by the lack of

1072 amplification with primer set A), while clone D2 likely had an insertion in protospacer site 12 as

1073 evidenced by a lack of amplification with primer set B. Clone F2 had amplification of the correct

1074 size at both protospacer sites (2 and 12), but we could not amplify the coding sequence from

1075 the F2 clone (right gel, lane labeled F2), suggesting that the locus was disrupted in this strain as

1076 well. All four of these knockout clones were assayed in biological triplicate for CCL22 induction

1077 in THP-1 cells (**Figure 3b**). B) Validation of 3 GRA4 knockout clones out of 5 tested. Clones

1078 A1:D6 and B2:C1 (where A1 and B1 indicate the parasites were from distinct transfections) had
1079 a likely insertion in the GRA4 gene at protospacer site 0, while clone B2:B11 had a likely
1080 insertion at both sites (0 and 26). C) Validation of 4 GRA8 knockout clones. Parasites were
1081 transfected with a single gRNA expressing plasmid (targeting gRNA sequence 4) and PCR on
1082 all 4 clones failed to amplify across the gRNA 4 target site. All amplifications across the gRNA
1083 target site 27 worked as did the positive control amplification of MAF1b. D) Validation of 4
1084 GRA28 knockout clones. Parasites were co-transfected with plasmids encoding gRNAs
1085 targeting sites 5 and 26 and queried using primers targeting the entire locus (sets A and B in
1086 this case), or flanking gRNA target sites 5 and 26 (sets C and D). PCR across the entire GRA28
1087 locus for clones 1A4, 1D4 and 1D3 all failed to generate PCR products, suggesting that these 3
1088 clones had disruptions in the *GRA28* gene. PCR on clone F3 with primer sets A and B gave a
1089 product of the expected size. PCR across the gRNA target site 26 failed for clone 1A4, while
1090 PCR across gRNA target site 5 failed for clones 1D4 and 1D3. Taken together these data
1091 indicate that clones 1A4, 1D4 and 1D3 were all GRA28 knockouts via insertion of selectable
1092 marker and accompanying plasmid sequences at the targeted gRNA sites. For clone 1F3 the
1093 locus seemed to be intact, but when we sequenced PCR products similar to those amplified by
1094 primer sets C and D (at gRNA target sites 5 and 26, respectively) we determined that clone 1F3
1095 had a single base pair deletion at base 250 relative to the start codon of GRA28 which
1096 introduced a stop codon 100 bp downstream of the indel (as well as multiple stop codons in
1097 frame further downstream). Sequences across the gRNA 26 target site were identical to wild
1098 type. The deletion near gRNA target site 5 was within the gRNA protospacer sequence itself,
1099 just proximal to the PAM site (GTTCCGCTGGTGCCTTCACC [TGG] was mutated to
1100 GTTCCGCTGGTGCCTT_ACC [TGG]). Therefore we treated 1F3 as a GRA28-null parasite
1101 strain. E) Validation of GRA18 knockouts received from the Bougdour lab: We received GRA18
1102 knockout and wild type clones from the laboratory of Alexandre Bougdour and validated them
1103 using PCR. In this case we generated primers to amplify across the entire GRA18 locus, which

1104 was completely deleted using double homologous recombination with large sequences flanking
1105 the entire coding region. As expected we could amplify across the entire GRA18 locus in
1106 PRU:WT and GRA18-complemented strains, but failed to do so in the GRA18 knockout.

1107

1108 **Figure 4 Supplementary Figure 1:** Ingenuity pathway analysis of THP-1 cells infected with
1109 RH:WT or RH Δ GRA28 *T. gondii* identifies candidate upstream regulatory gene products that
1110 may be driving GRA28-dependent differences in transcript abundance. A) Genes of higher
1111 abundance in RH:WT-infected THP-1 cells were found to be significantly associated with
1112 multiple immunity-related regulatory genes, including those related to the NF κ B pathway (e.g.,
1113 NF κ BIA, NF κ B1 and REL). B) Hierarchical cluster of correlations in the amount of target gene
1114 overlap for each of the upstream regulators shown in A. A small cluster of the most highly
1115 correlated genes contained multiple genes relevant to NF κ B activation (outlined in dotted
1116 green). C) As in B, most of the upstream regulators had the same downstream targets, and this
1117 was most evident for the AP-1 transcription factor complex (encoded by *FOS* and *JUN* genes)
1118 as well as *IL1B* and *ICAM1*. A heat map indicating fold-differences between RH:WT and
1119 RH Δ GRA28-infected THP-1 cells for these downstream targets is also shown. D) Heatmap
1120 showing transcript abundance for all transcriptional regulators that were found to be significantly
1121 altered in infected THP-1 cells in a GRA28-dependent manner ($P < 0.001$; $\log_2(\text{fold-}$
1122 $\text{difference}) \geq 1$).

1123

1124 **Figure 4 Supplementary Figure 2:** C-JUN protein levels are induced by *T. gondii* infection in
1125 THP-1 cells but do not depend on the presence or GRA28 in the infecting strain. THP-1 cells
1126 were infected with the indicated strains (or mock-treated by exposing them to the same WT
1127 parasite suspensions as for infection but after sterile-filtering with a 0.2 μm filter) for 24 h and
1128 then C-JUN protein level was quantified using western blotting. Histone H3 levels served as a
1129 control and densitometry was used to calculate the C-JUN/Histone H3 ratio as a proxy for

1130 normalized C-JUN abundance. Two replicates, with an N=3 wells of cells for infections and N=2
1131 wells for mock, are shown, each having similar results.

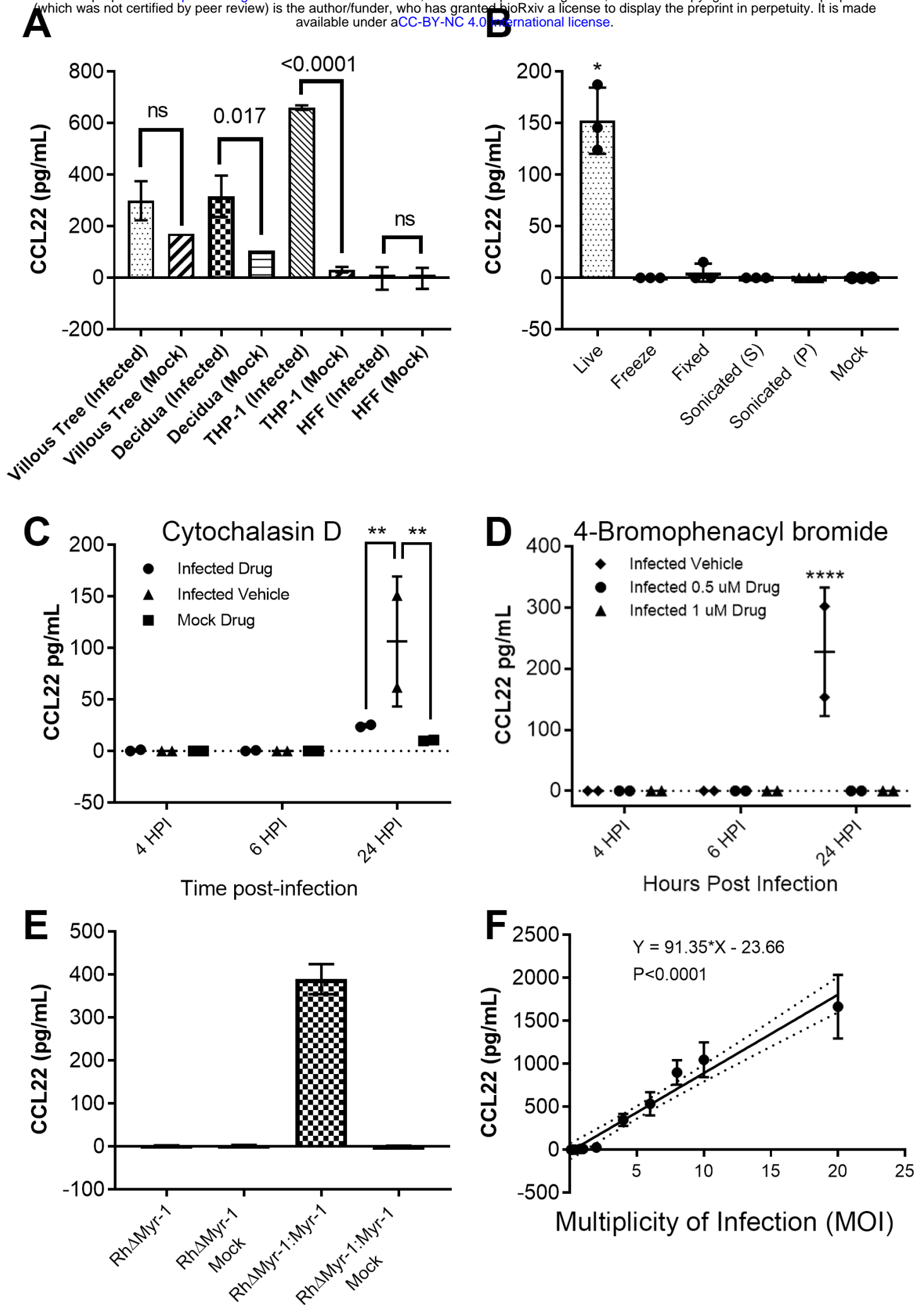
1132

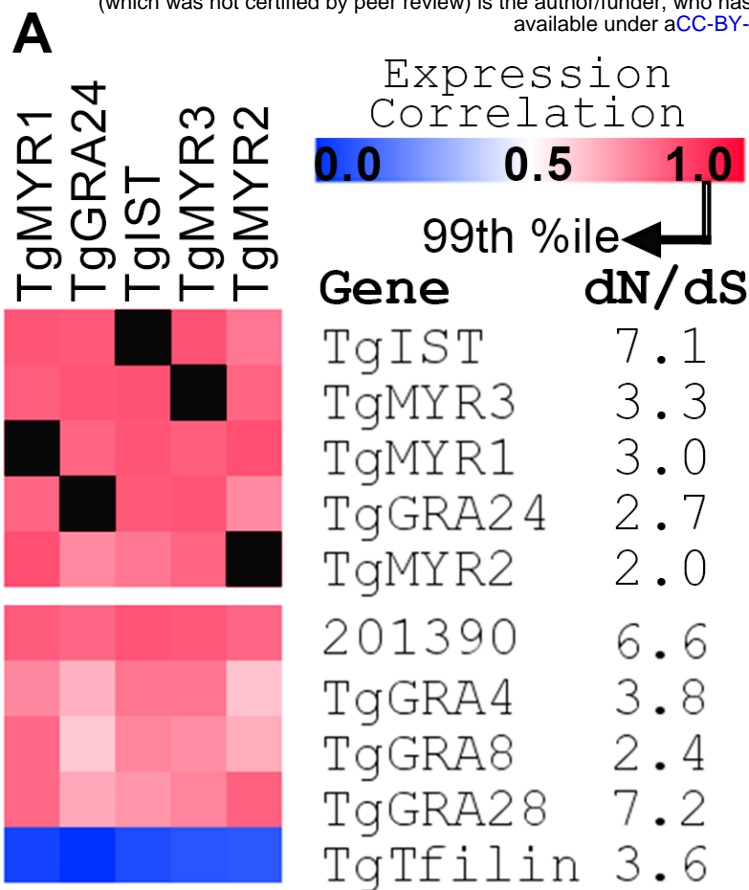
1133 **Figure 5 Supplementary Figure 1:** A) Quantification of nuclear localization in *T. gondii* (N=5)
1134 and *N. caninum* (N=3) vacuoles expressing Exon 1 of *T. gondii* HA-tagged GRA28. Data were
1135 normalized for each image and HA-positive vacuole by subtracting mean HA-intensity in a
1136 nucleus neighboring the infected cell from the mean GFP intensity in the nucleus of the infected
1137 cell, and then dividing that by the mean HA-intensity of the parasite-containing vacuole.
1138 Expression in *T. gondii* led to significantly ($P < 0.01$; T-test on the log₁₀-normalized data) higher
1139 normalized intensity in the nucleus compared to when GRA28 was expressed in *N. caninum*.
1140 B,C) Schematic illustrating how data in A were collected and calculated for *T. gondii* (B) and *N.*
1141 *caninum* (C).

1142

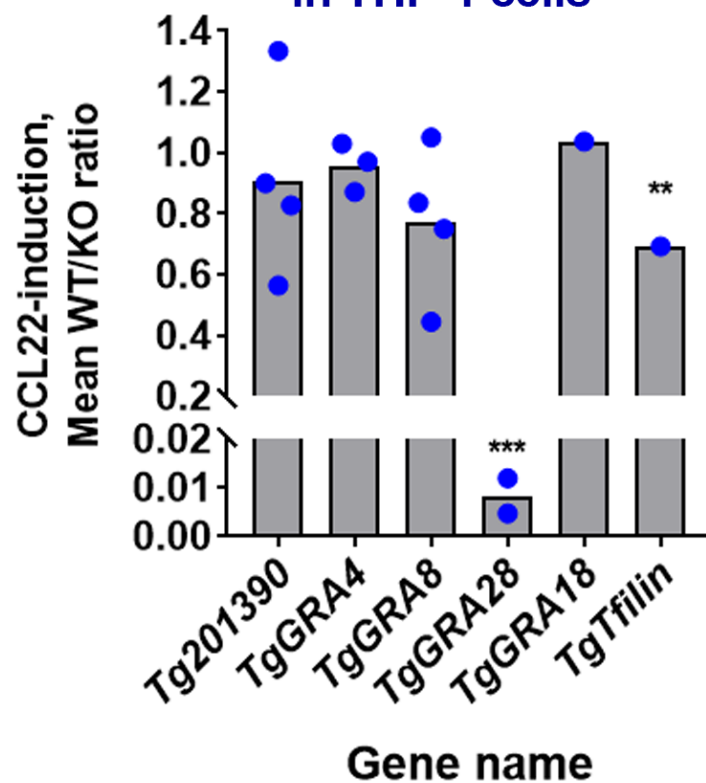
1143 **Figure 7 Supplementary Figure 1:** Visual representation of pathology index scores. All images
1144 are the same individual from two viewpoints (lateral and dorsal) at four different timepoints of
1145 infection. **0)** No fur ruffling or red/irritated skin present. **1)** Mild ruffling present predominantly
1146 located on the head and back of the neck. No red/irritated skin visible. **2)** Moderate ruffling
1147 present - fur forms larger clumps and extends to the rest of the body. Skin may be visible
1148 through the clumps but is not red or irritated. **3)** Severe ruffling is characterized by ruffling
1149 across the entire body with visibly red/irritated skin.

1150

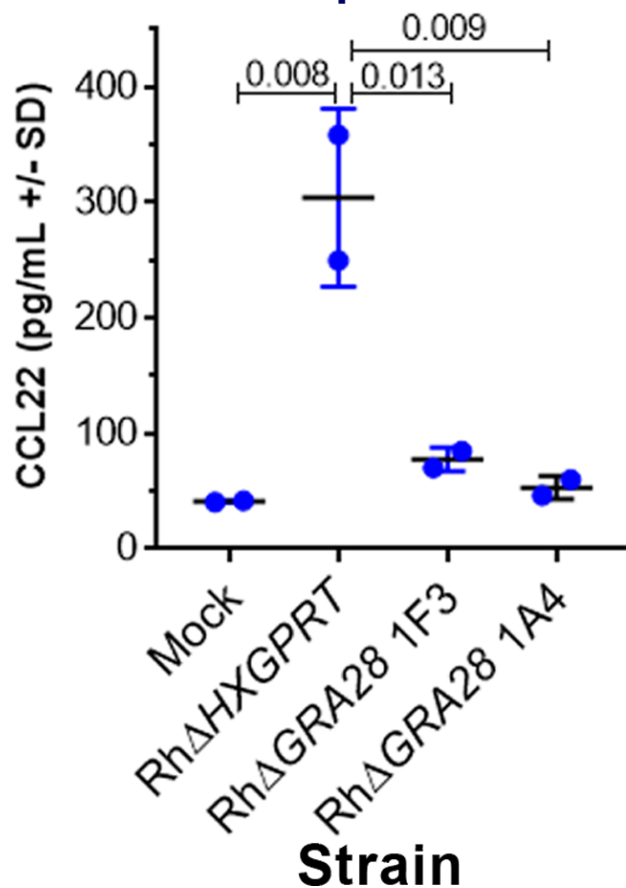




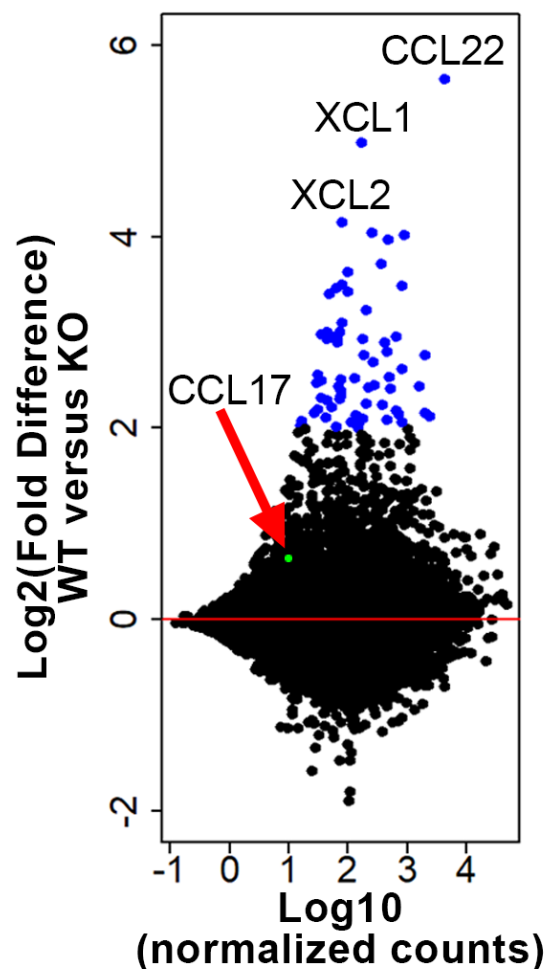
B Knockouts screened in THP-1 cells

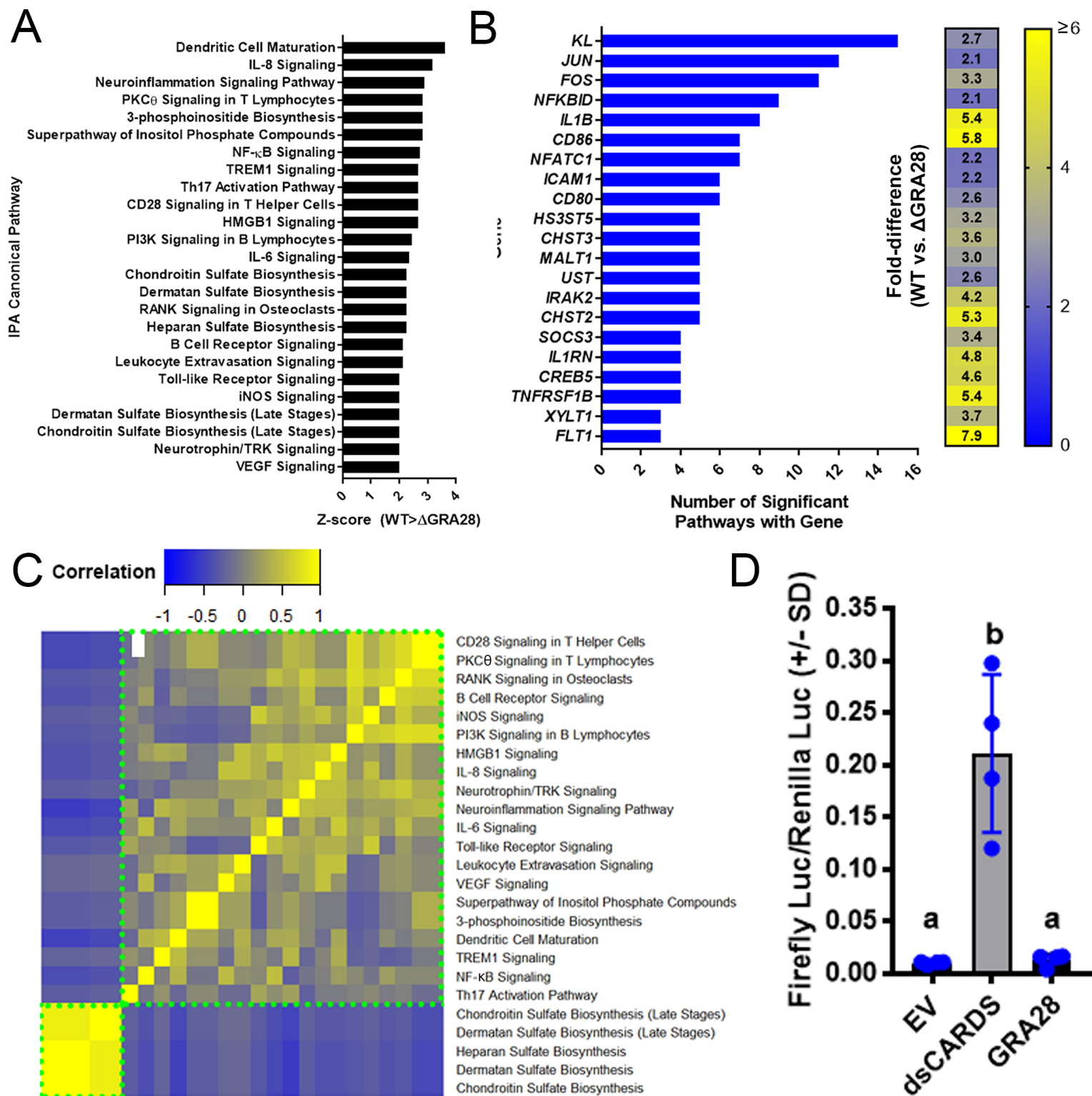


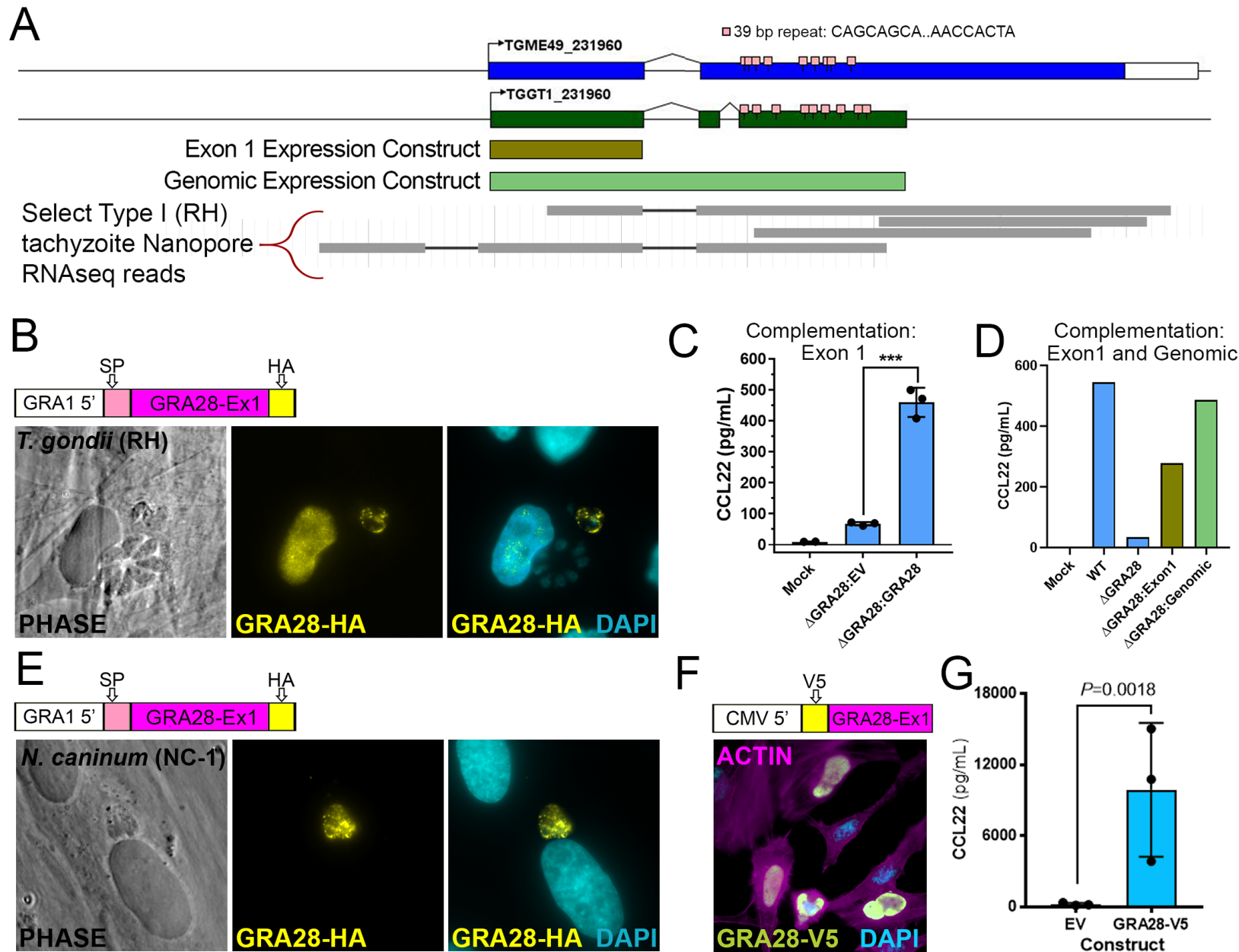
C Human Placental Explants

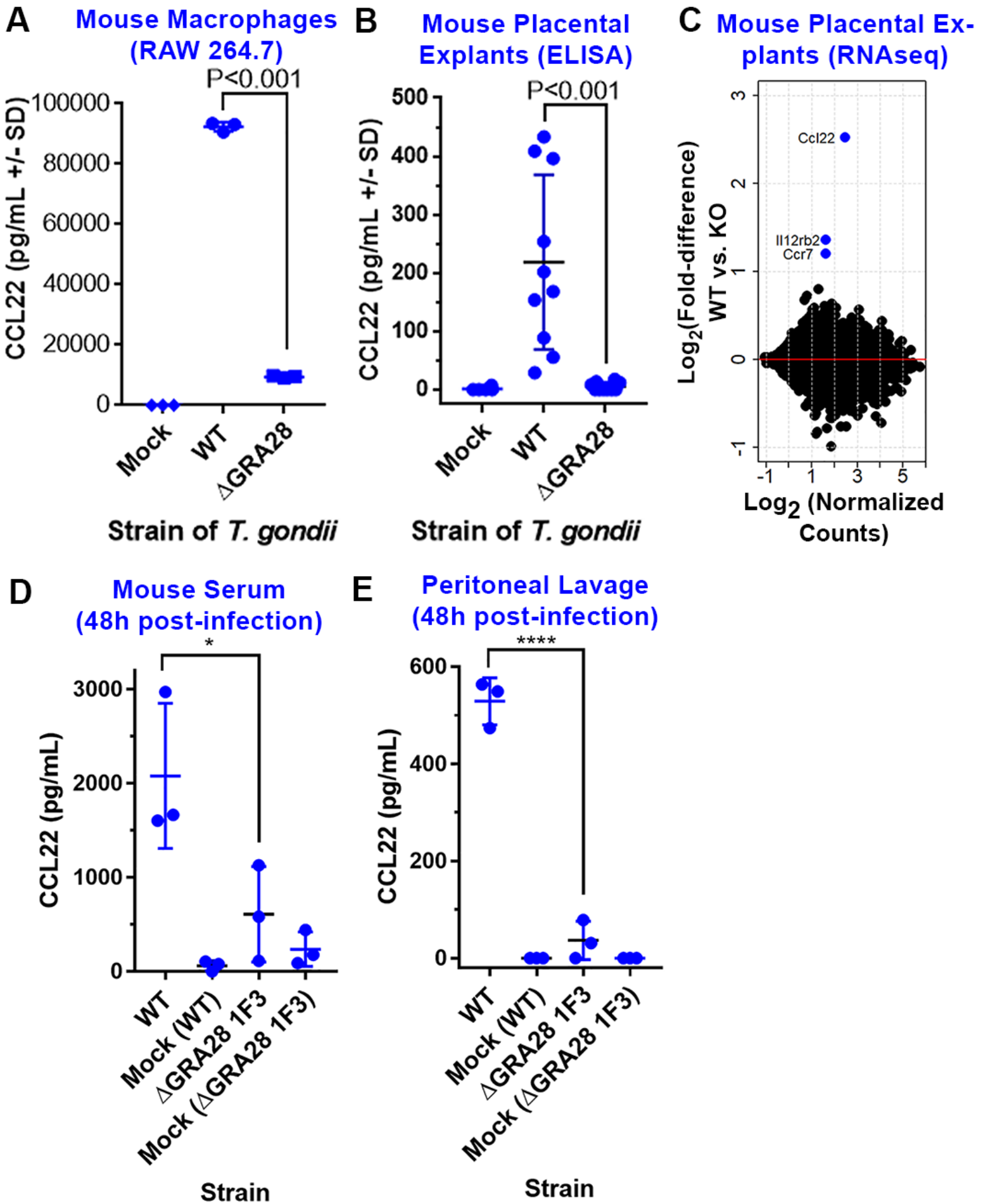


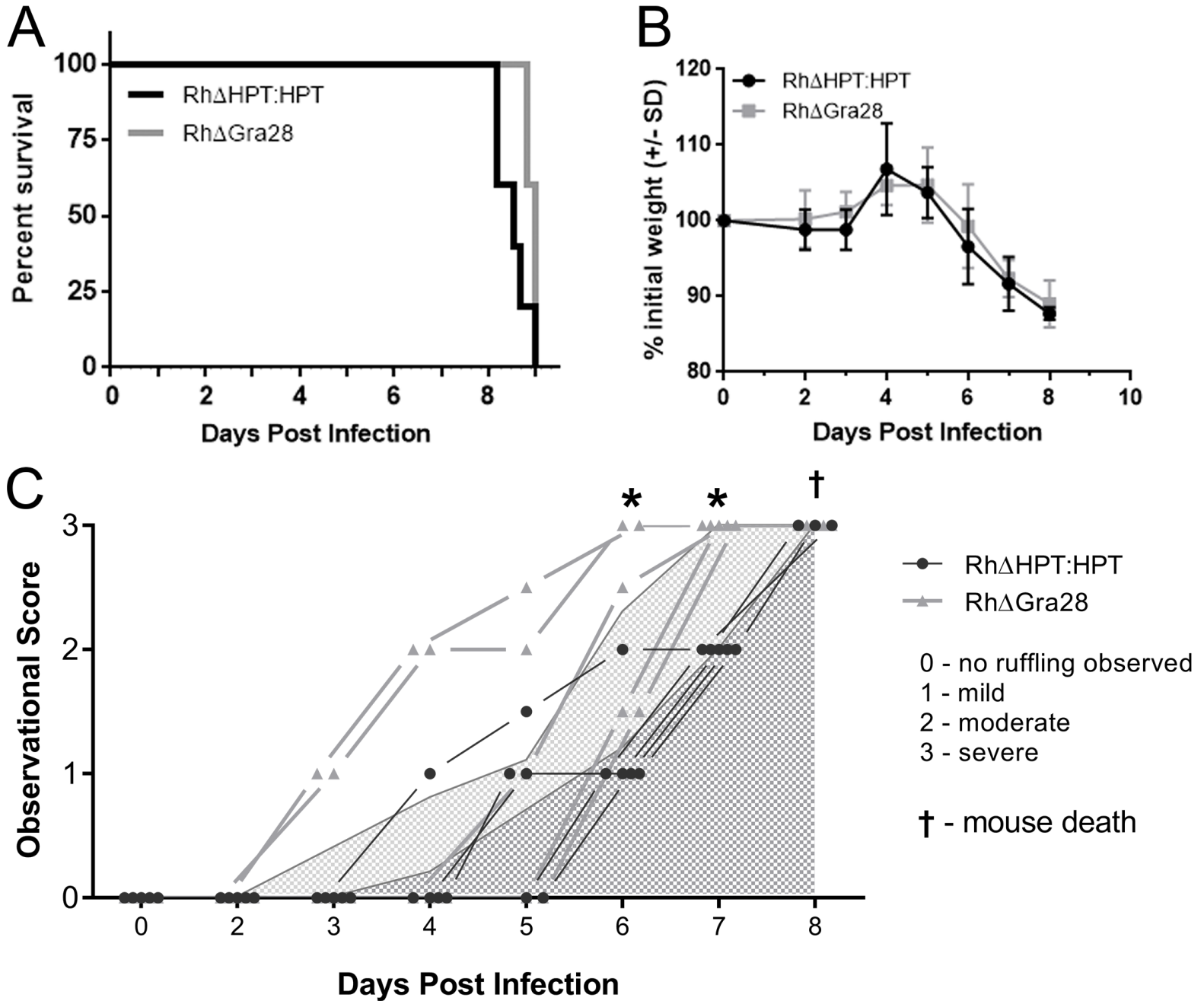
D



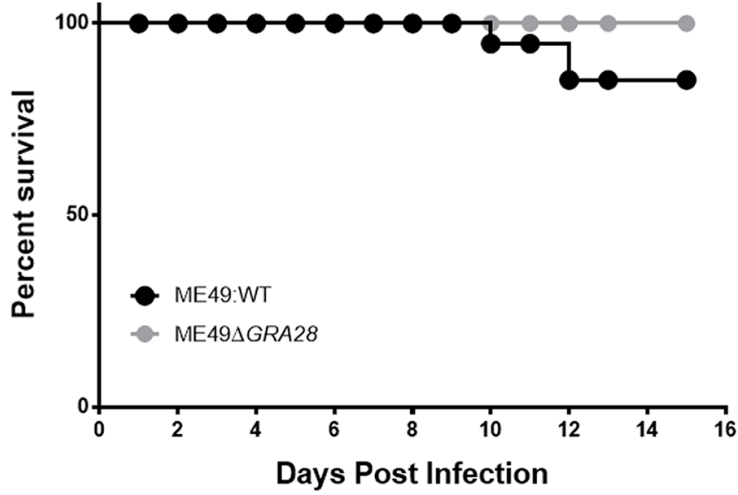




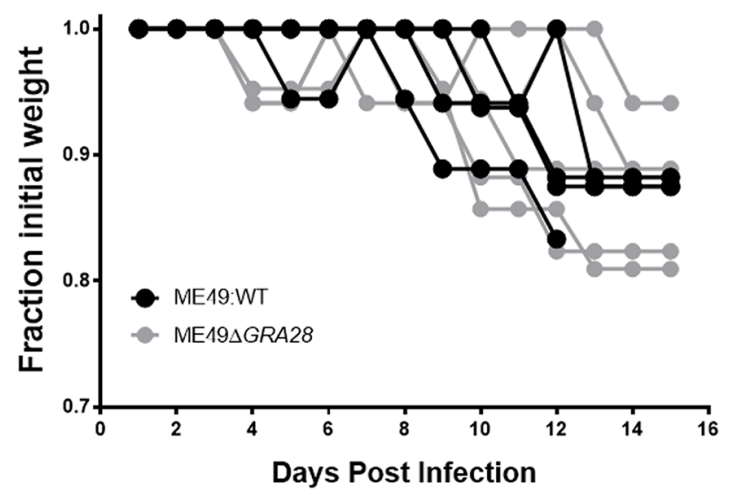




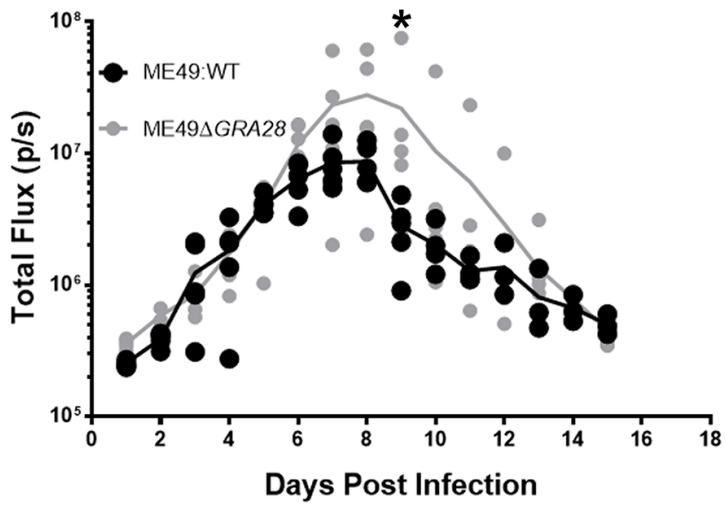
A



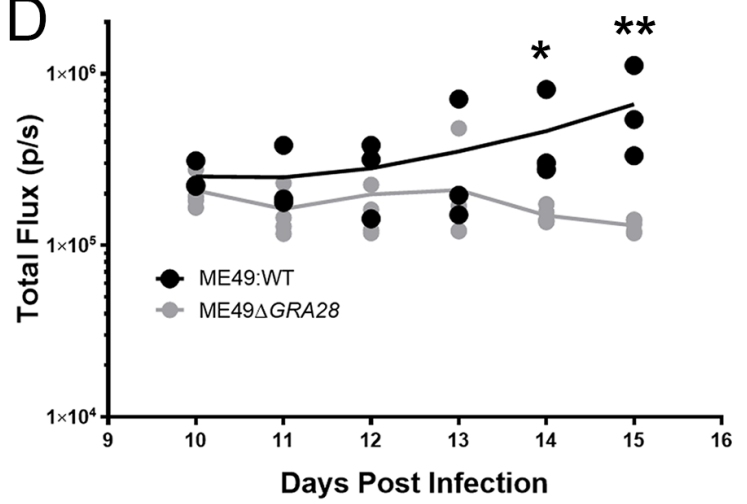
B



C



D



E

